A Newton - Galerkin Finite Element Method to solve reduced dimensional Variable Density Flow and Solute Transport Equations using Proper Orthogonal Decomposition Method

by

Olcay Ciftci

A dissertation submitted to the Graduate Faculty of
Auburn University
in partial fulfillment of the
requirements for the Degree of
Doctor of Philosophy

Auburn, Alabama
August 8

Keywords: Proper Orthogonal Decomposition, Variable Density Flow and Solute Transport Equations

Approved by

Yanzhao Cao, Chair, Professor of Mathematics and Statistics
Hans Werner van Wyk, Co-Chair, Assistant Professor of Mathematics and Statistics
Dmitry Glotov, Associate Professor of Mathematics and Statistics
Erkan Nane, Associate Professor of Mathematics and Statistics
Junshan Lin, Associate Professor of Mathematics and Statistics

Abstract

The mathematical model of Variable Density Flow and Solute Transport (VDFST) is a time dependent, coupled and nonlinear dynamical system that is widely used to simulate sea-water intrusion and related problems. The numerical problem is relatively easy to solve when the transport of solute does not affect fluid density, but when there are big differences in density, the problem of solute transport is much more difficult to solve because of the high degree of nonlinearity. The numerical discretizations of VDFST in time and space are usually required to be as fine as possible, but due to their high dimensional structure there is a strong need to reduce the computational costs and storage requirements. Proper orthogonal decomposition (POD), as a model order reduction (MOR) technique, aims to lower the computational complexity by approximating the large-scaled discretized state equations using a low-dimensional model. POD is an effective numerical technique to reduce the computational cost for state estimation, forward prediction and inverse modeling.

In this research, POD was used with the Galerkin finite element method (GFEM) and the Newton iteration approach to reduce the computational time and the relative error between the results we obtain from the reduced dimensional and high dimensional models of VDFST. The modified Henry problem and Elder problem were used to demonstrate the capability of the model. It was showed that the reduced dimensional model that was solved with Newton iteration approach can reproduce and predict the full model results very accurately with much less computational time in comparison with the full dimensional model and the reduced dimensional model that was solved with coupling iteration approach.

Acknowledgments

I am truly grateful to my advisors, Dr. Yanzhao Cao and Dr. Hans Werner van Wyk, for their thoughtful suggestions, support, understanding, encouragement, and patience throughout this dissertation process. I really appreciate their prompt assistance with invaluable advices on this dissertation. This dissertation would never be complete without them.

Besides my advisors, I would like to thank Dr. Erkan Nane, Dr. Dmitry Glotov and Dr. Junshan Lin for becoming my PhD dissertation committee members. I got many ideas from their classes.

My special thank goes to my family: my parents, my wife, my children and my brothers, for their endless encouragement, warm support, and unconditional love.

Thanks again to all who helped me.

Table of Contents

List of Figures

List of Tables

Chapter 1

INTRODUCTION

Large-scale, high-dimensional dynamical systems are often given by discretization of systems of nonlinear partial differential equations. In many fields of science and engineering, these dynamical systems need to be simulated, optimized or controlled, but due to their high dimensional structure there is a strong need to reduce the computational costs and storage requirements. Model order reduction (MOR) techniques aim to lower the computational complexity by approximating the large-scaled discretized state equations using low-dimensional model. Reduced order model methods that are most frequently used today can be widely categorized into four groups: Proper orthogonal decomposition (POD) methods, reduced basis methods, balancing methods, simplified physics or operational based reduction methods.

Hydrology is one the science fields where MOR techniques are commonly used. Simulating the natural system using the numerical models is a significant challenge for ground water modelers, since they consist of large model networks which describe the reality more and more. In the last decade, Vermeulen et al. [61, 62, 63, 64, 65, 66] has analyzed, developed and implemented MOR methods for subsurface flow equations. In these studies, a low-dimensional formulation for groundwater flow that reduces the computational burden necessary for inverse modeling was described. In other studies [12, 16, 36, 37, 55, 63], POD, as a common MOR technique, was applied to subsurface flow problems.

POD, also known as Karhunen - Loéve (K - L) expansion or principle components analysis, was first introduced by Lumley [38] to identify coherent structures in dynamical systems. In recent years, the technique has been widely used in studies and implemented effectively to a variety of fields such as control problems, inverse problems, image processing, signal

analysis, pattern recognition, data compression, oceanography, and fluid mechanics. POD is an effective numerical technique to reduce the computational cost for state estimation, forward prediction and inverse modeling. The primary goal in POD is to obtain optimal low dimensional basis for representing a set of high-dimensional experimental or simulation data [30, 31, 36, 37, 46, 55, 66]. Each basis, known by several names such as POD basis, proper orthogonal modes (POM), empirical eigenfunctions or empirical orthogonal functions, is associated with a certain amount of variance or energy.

Although there are some groundwater-related problems that can be solved by a single flow model, they are limited. In practice, coupled models like VDFST are more involved for complicated groundwater processes. The numerical problem is relatively easy to solve when the transport of solute does not affect fluid density, since flow and transport are not coupled. However, when there are big differences in density, the problem of solute transport is much more difficult to solve because of the high degree of nonlinearity. Indeed, when salt water is involved, the fluid density variations affect the local velocity field. Such nonlinearity can cause recirculation regions and makes the solute distribution in the domain difficult to predict.

VDFST is a coupled nonlinear dynamical system that is widely used to simulate seawater intrusion and related problems [8, 17, 23, 36, 37, 68, 69]. Due to the coupling process, the governing equations must be solved simultaneously. Although the finite difference method (FD) method is usually used to solve a single flow model, the Galerkin finite element method (GFEM) is often adopted to solve VDFST models.

In a study, Li et al. [36, 37] developed a GFEM-POD reduced-order method to transform the VDFST model into reduced dimensional form, and then using a coupling iteration approach the high-dimensional model simulation results were approximately reproduced with a significant time and computational complexity reduction. The modified Henry Problem [24, 59] and Elder problem [19, 20] were used to check the efficiency of the method. In the study, firstly solute concentration and fresh water hydraulic head snapshots (a set of data of state variables) were collected by simulating the original high dimensional model, and then singular value decomposition (SVD) was applied to the ensemble of snapshots separately to obtain a set of POD modes that span the snapshot collection. Using these POD bases and Galerkin projection, a

set of reduced dimensional coupled ODEs derived. Then, the system was solved with coupling iteration to find the time coefficients that are used to reproduce the state variables for any time any location in the domain.

In this dissertation, GFEM-POD method was used with Newton iteration to reduce the computational time and the relative error between the results we obtain from the reduced dimensional and high dimensional models. The modified Henry problem and Elder problems were used to demonstrate the capability of the model.

This dissertation is organized as follows. In Chapter 2, the formulation of variable density flow and solute transport model is introduced. In Chapter 3, GFEM is applied to solve discretized mathematical model. Application of POD on VDFST to obtain a reduced dimensional model is demonstrated in Chapter 4 with an error analysis. In Chapter 5, the developed method is applied to two benchmark problems to check the accuracy and efficiency of the method. Finally, in Chapter 6, some conclusion remarks are provided based on the results.

Chapter 2

VARIABLE DENSITY FLOW AND SOLUTE TRANSPORT EQUATIONS (VDFST)

2.1 Concept of Head and Equivalent Freshwater Head

Hydraulic head is one of the important variables which is used to describe a groundwater system. It is calculated as the sum of a pressure term, an elevation term, and a kinetic energy term. Since the groundwater velocities are so slow, kinetic energy is typically negligible, and hydraulic head is usually evaluated as the sum of the pressure and elevation terms.

To measure head and equivalent freshwater head, two piezometers which are shown in Figure 2.1 are located to a specific point, N, in a porous aquifer that contains saline water [23]. Piezometer A contains saline water that is identical to the aquifer water at point N. The elevation of the water level in piezometer A is $P_N/\rho g$, and head at the point N is the height of the water level in the piezometer above datum which is calculated by $h = \frac{P_N}{\rho g} + Z_N$ where P_N is the pressure at the point N, ρ is the fluid density, g is gravitational acceleration and Z_N is the elevation of the point N above the datum. Piezometer B contains freshwater and has a mechanism to prevent saline water in the aquifer from mixing with freshwater in the piezometer. This mechanism also allows the piezometer to respond accurately to the pressure at the point N. Similarly, the elevation of the water level in piezometer B is $P_N/\rho_f g$, and head at the point N is the height of the water level in the piezometer above datum which is calculated by $h_f = \frac{P_N}{\rho_f g} + Z_N$ where P_N is the pressure at the point N, ρ_f is the freshwater density, g is gravitational acceleration and Z_N is the elevation of the point N above the datum. The head h_f is called equivalent freshwater head.

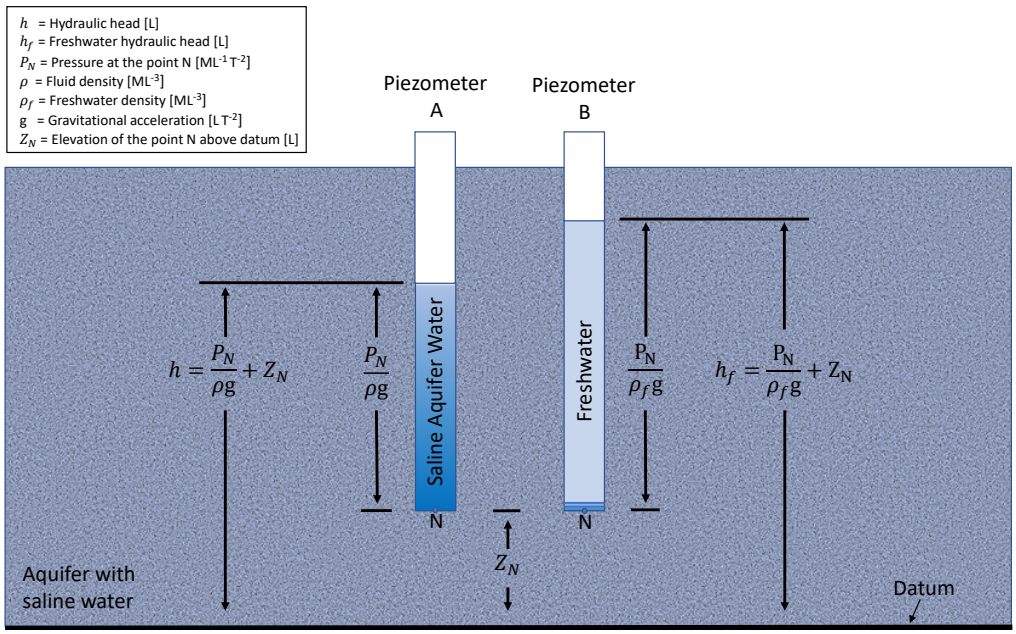

Figure 2.1 Piezometer A filled with saline aquifer water and B with freshwater, open to the same point in the aquifer.

2.2 Governing Equations for Flow and Transport

2.2.1 Variable density Ground-Water Flow Equation

The law of conservation of mass or principle of mass conservation is one of the most fundamental principles in nature and widely used in many fields such as fluid dynamics, mechanics and chemistry. The law states that the rate of accumulation of mass stored in a control volume (CV) is equal to the algebraic sum of the mass fluxes across the faces of the CV and the mass exchange due to sinks or sources. The mass-balance equation for the water (ignoring dispersion) can be expressed mathematically as follows [23]:

$$\frac{\partial}{\partial t}(\theta\rho) = -\nabla \cdot (\rho \mathbf{q}) + \rho_R Q_R - \rho Q_P, \tag{2.1}$$

where:

∇ is the gradient operator $(\frac{\partial}{\partial x})\hat{\mathbf{i}} + (\frac{\partial}{\partial y})\hat{\mathbf{j}} + (\frac{\partial}{\partial z})\hat{\mathbf{k}}$,

ρ is the fluid density $[ML^{-3}]$,

$\mathbf{q}$ is the specific discharge vector $[LT^{-1}]$,

θ is effective porosity [dimensionless],

Q_R and Q_P are injection/removal rates $[LT^{-1}]$,

ρ_R is fluid density of source $[ML^{-3}]$

To derive the flow equation, firstly, the left-hand side of the equation (2.1) is expanded as:

$$\frac{\partial}{\partial t}(\theta\rho) = \rho\frac{\partial\theta}{\partial t} + \theta\frac{\partial\rho}{\partial t}. \tag{2.2}$$

where $\theta = \theta(P)$ and $\rho = \rho(P, C)$. Since the changes of fluid pressure affect the effective porosity it can be written as a function of fluid pore pressure. Similarly, the fluid density can be evaluated as a function of fluid pore pressure and solute concentration under isothermal conditions. The change of effective porosity and density with time can be expressed as [23]:

$$\frac{\partial\rho}{\partial t} = \frac{\partial\rho}{\partial P}\frac{\partial P}{\partial t} + \frac{\partial\rho}{\partial C}\frac{\partial C}{\partial t}. \tag{2.3}$$

and

$$\frac{\partial\theta}{\partial t} = \frac{\partial\theta}{\partial P}\frac{\partial P}{\partial t}. \tag{2.4}$$

Substituting the equations (2.3) and (2.4) into the equation (2.2) the following equation can be derived [23]:

$$\frac{\partial}{\partial t}(\theta\rho) = \rho\frac{\partial\theta}{\partial t} + \theta\frac{\partial\rho}{\partial t} = \rho\frac{\partial\theta}{\partial P}\frac{\partial P}{\partial t} + \theta\frac{\partial\rho}{\partial P}\frac{\partial P}{\partial t} + \theta\frac{\partial\rho}{\partial C}\frac{\partial C}{\partial t}. \tag{2.5}$$

The relation between water compressibility, fluid density and pressure is shown as [7]:

$$\frac{\partial\rho}{\partial P} = \rho\zeta, \tag{2.6}$$

where ζ is the coefficient of water compressibility $[M^{-1}LT^2]$. The relation between pressure, porosity and the compressibility of a bulk porous material is defined as [7]:

$$\frac{\partial\theta}{\partial P} = (1-\theta)\xi, \tag{2.7}$$

where ξ is the compressibility of the bulk porous material $[M^{-1}LT^2]$. Substituting the equations (2.6) and (2.7) into the equation (2.5) the following equation can be written [23]:

$$\frac{\partial}{\partial t}(\theta\rho) = \rho(1-\theta)\xi\frac{\partial P}{\partial t} + \theta\rho\zeta\frac{\partial P}{\partial t} + \theta\frac{\partial \rho}{\partial C}\frac{\partial C}{\partial t}. \tag{2.8}$$

Rearranging the equation (2.8), and then substituting it in the equation (2.1) the following equation is derived

$$\rho S_p\frac{\partial P}{\partial t} + \theta\frac{\partial \rho}{\partial C}\frac{\partial C}{\partial t} = -\nabla\cdot(\rho\mathbf{q}) + \rho_R Q_R - \rho Q_P \tag{2.9}$$

where $S_p = \zeta\theta + \xi[1-\theta]$ is the specific storage in terms of pressure. The equivalent freshwater head at the piezometer B shown in Figure 2.1 is the elevation of the water level in piezometer above datum and expressed as:

$$h_f = \frac{P}{\rho_f g} + z \tag{2.10}$$

Rearranging the equation (2.10), the following expression can be derived:

$$P = \rho_f g(h_f - z) \tag{2.11}$$

Differentiating the equation (2.11) with respect to time, the change of pressure in time can be written as:

$$\frac{\partial P}{\partial t} = \rho_f g\frac{\partial h_f}{\partial t} \tag{2.12}$$

Substituting the equation (2.12) into the equation (2.9), flow equation can be expressed as:

$$\rho S_p\rho_f g\frac{\partial h_f}{\partial t} + \theta\frac{\partial \rho}{\partial C}\frac{\partial C}{\partial t} = -\nabla\cdot(\rho\mathbf{q}) + \rho_R Q_R - \rho Q_P \tag{2.13}$$

Neglecting the difference between the compressibility coefficients of saltwater (ζ) and freshwater (ζ_f) such that $\zeta \approx \zeta_f$, the expression in the equation (2.13) can be written as:

$$g\rho_f S_p = S_f \tag{2.14}$$

where S_f $[L^{-1}]$ is the specific storage in terms of freshwater head.

Substituting the equation (2.14) into (2.13) yields to:

$$\rho S_f \frac{\partial h_f}{\partial t} + \theta \frac{\partial \rho}{\partial C} \frac{\partial C}{\partial t} = -\nabla \cdot (\rho \mathbf{q}) + \rho_R Q_R - \rho Q_P \tag{2.15}$$

2.2.2 Darcy's Law

Darcy's law is an equation that shows the volumetric flow rate as a function of the flow area, fluid pressure, elevation and a proportionality constant. It is stated in several different forms depending on the flow conditions. The general form of Darcy's law for a fluid of variable density can be defined as [45]:

$$\mathbf{q} = -\frac{\mathbf{k}}{\mu} (\nabla P + \rho g \nabla z) \tag{2.16}$$

where:

μ is dynamic viscosity,

z is the elevation of the point of measurement above some datum

∇z is the unit vector in the vertical (z) direction,

g is acceleration due to gravity,

P is pressure,

$\mathbf{k}$ is permeability tensor

To write the equation (2.16) in another form, firstly, we differentiate the equation (2.11) and derive the following expression:

$$\nabla P = \rho_f g \nabla h_f - \rho_f g \nabla z \tag{2.17}$$

Then, substituting (2.17) into the equation (2.16), the following mathematical expression is written:

$$\mathbf{q} = -\frac{\mathbf{k} \rho_f g}{\mu} \left(\nabla h_f + \frac{\rho - \rho_f}{\rho_f} \nabla z \right) \tag{2.18}$$

The freshwater hydraulic conductivity tensor, $\mathbf{K_f}$, is defined as:

$$\mathbf{K_f} = \frac{\mathbf{k}\rho_f g}{\mu_f} \tag{2.19}$$

where μ_f is the freshwater fluid viscosity.

In the literature, there are several basic examples of constitutive equations that show the relation between the density and concentration. In this dissertation, we focus on the linear case shown as:

$$\rho = \rho_f + EC \tag{2.20}$$

where $E = \frac{\partial \rho}{\partial C}$ is a dimensionless constant. Rewriting the equation (2.20), the following expression can be obtained:

$$\frac{\rho - \rho_f}{\rho_f} = \eta C \tag{2.21}$$

or

$$\frac{\rho}{\rho_f} = 1 + \eta C \tag{2.22}$$

where $\eta = \frac{E}{\rho_f}$. Substituting the equations (2.19) and (2.21) into (2.18), the specific discharge vector $\mathbf{q}$ can be expressed as:

$$\mathbf{q} = -\mathbf{K_f}\frac{\mu_f}{\mu}\left(\nabla h_f + \eta C \nabla z\right) \tag{2.23}$$

2.2.3 Governing Equation for Flow

For many applications, the ratio of the freshwater and saltwater fluid viscosity, $\frac{\mu_f}{\mu}$, is considered equal one. Substituting the equation (2.23) into the equation (2.15) and assuming $\frac{\mu_f}{\mu} = 1$, the following expression is derived [7, 23, 45]:

$$\rho S_f \frac{\partial h_f}{\partial t} + \theta E \frac{\partial C}{\partial t} = \nabla \cdot \Big(\rho \mathbf{K_f}\big[\nabla h_f + \eta C \nabla z\big]\Big) + \rho_R Q_R - \rho Q_P \tag{2.24}$$

where $E = \frac{\partial \rho}{\partial C}$. Dividing both side of the equation (2.24) by ρ_f yields the equation:

$$\frac{\rho}{\rho_f} S_f \frac{\partial h_f}{\partial t} + \theta \frac{E}{\rho_f} \frac{\partial C}{\partial t} = \nabla \cdot \Big(\frac{\rho}{\rho_f} \mathbf{K_f} \big[\nabla h_f + \eta C \nabla z \big] \Big) + \frac{\rho_R}{\rho_f} Q_R - \frac{\rho}{\rho_f} Q_P \tag{2.25}$$

Since $\frac{\rho}{\rho_f} = 1 + \eta C$ and $\eta = \frac{E}{\rho_f}$, the equation (2.25) can be written as:

$$(1 + \eta C) S_f \frac{\partial h_f}{\partial t} + \theta \eta \frac{\partial C}{\partial t} = \nabla \cdot \Big((1 + \eta C) \mathbf{K_f} \big[\nabla h_f + \eta C \nabla z \big] \Big) + \frac{\rho_R}{\rho_f} Q_R - (1 + \eta C) Q_P \tag{2.26}$$

Equation (2.26) is the governing equation for flow in terms of freshwater head.

2.2.4 Governing Equation for Solute Transport

Since the redistribution of solute concentration affects the density fields during the groundwater flow, a second governing equation for the transport of solute mass in the porous aquifer is required. The law of the conservation of mass for concentration can be written as [7, 23, 45]:

$$\theta \frac{\partial C}{\partial t} = \nabla \cdot (\theta \mathbf{D} \nabla C) - \nabla C \cdot \mathbf{q} + C_R Q_R - C Q_P, \tag{2.27}$$

where:

∇ is the gradient operator $(\frac{\partial}{\partial x})\hat{\mathbf{i}} + (\frac{\partial}{\partial y})\hat{\mathbf{j}} + (\frac{\partial}{\partial z})\hat{\mathbf{k}}$,

C is fluid concentration $[ML^{-3}]$

$\mathbf{D}$ is the hydrodynamic dispersion coefficient $[L^2T^{-1}]$,

$\mathbf{q}$ is the specific discharge vector $[LT^{-1}]$,

θ is effective porosity [dimensionless],

Q_R and Q_P are injection/removal rates $[LT^{-1}]$,

C_R is fluid concentration of source $[ML^{-3}]$

Substituting the equation (2.23) into the equation (2.27), and then dividing both side of the equation by θ assuming $\frac{\mu_f}{\mu} = 1$, the following equation is derived:

$$\frac{\partial C}{\partial t} = \nabla \cdot (\mathbf{D} \nabla C) + \nabla C \cdot \frac{\mathbf{K}_f}{\theta} (\nabla h_f + \eta C \nabla z) + \frac{C_R}{\theta} Q_R - \frac{C}{\theta} Q_P \tag{2.28}$$

which is the governing equation for solute transport in porous medium.

2.2.5 Governing System of VDFST Equations

Let Ω be the bounded calculation spatial domain and T be the time period of calculation. The final system of equations in terms of the state variables h_f and C that we will use in our model can be described as:

Flow equation:

$$\begin{aligned}(1+\eta C)S_f\frac{\partial h_f}{\partial t}+\theta\eta\frac{\partial C}{\partial t}&=\nabla\cdot\Big((1+\eta C)\mathbf{K_f}\big[\nabla h_f+\eta C\nabla z\big]\Big)+\frac{\rho_R}{\rho_f}Q_R-(1+\eta C)Q_P\\ \mathbf{x}\in\Omega\quad 0\le t\le T&\end{aligned}\tag{2.29}$$

with the following initial and boundary conditions:

$h_f(\mathbf{x},0)=h_f^0(\mathbf{x})\quad \mathbf{x}\in\Omega$

$h_f(\mathbf{x},t)|_{\Gamma_D^{h_f}}=h_f^1(\mathbf{x})\quad \mathbf{x}\in\Gamma_D^{h_f}$

$\big((1+\eta C)\mathbf{K}\left(\nabla h_f+\eta C\nabla z\right)\big)\cdot\mathbf{n}|_{\Gamma_N^{h_f}}=\rho_q q(\mathbf{x},t)\quad \mathbf{x}\in\Gamma_N^{h_f}$

where,

$\Gamma_D^{h_f}$: Dirichlet Boundary Condition for h_f

$\Gamma_N^{h_f}$: Neumann Boundary Condition for h_f

Solute Transport equation:

$$\begin{aligned}\frac{\partial C}{\partial t}=&\quad\nabla\cdot(\mathbf{D}\nabla C)+\nabla C\cdot\frac{\mathbf{K}_f}{\theta}\left(\nabla h_f+\eta C\nabla z\right)+\frac{C_R}{\theta}Q_R-\frac{C}{\theta}Q_P\\ \mathbf{x}\in\Omega\quad 0\le t\le T&\end{aligned}\tag{2.30}$$

with the following initial and boundary conditions:

$C(\mathbf{x},0)=C^0(\mathbf{x})\quad \mathbf{x}\in\Omega$

$C(\mathbf{x},t)|_{\Gamma_D^C}=C^1(\mathbf{x})\quad \mathbf{x}\in\Gamma_D^C$

$\big(\mathbf{D}\nabla C\big)\cdot\mathbf{n}|_{\Gamma_N^C}=g(\mathbf{x},t)\quad \mathbf{x}\in\Gamma_N^C$

where,

Γ_D^C : Dirichlet Boundary Condition for C

Γ_N^C : Neumann Boundary Condition for C

Chapter 3

NUMERICAL METHODS FOR VDFST

3.1 Weak Formulation

In this section, the weak formulation of the VDFST equations is developed. The space $H^1(\Omega)$ is the standard Sobolev space of order one, and the notation $\langle \cdot, \cdot \rangle_\Omega$ is defined as the standard inner product over $L_2(\Omega)$ as $\langle f, g \rangle_\Omega = \int_\Omega fg \, d\Omega$ with L_2 norm $||f|| = \langle f, f \rangle^{1/2}$.
Let $V_0^{h_f} = \{v \in H^1(\Omega) : v|_{\Gamma_D^{h_f}} = 0\}$ and $V_0^C = \{v \in H^1(\Omega) : v|_{\Gamma_D^C} = 0\}$.
Multiplying the equations (2.29) and (2.30) by test functions $\phi^{h_f} \in V_0^{h_f}$ and $\phi^C \in V_0^C$, respectively, integrating over the spatial domain, Ω, and integrating by parts with boundary conditions gives the following abstract variational problem [45]: Find solutions $h_f, C \in H^1(\Omega)$ such that:

$$\begin{aligned}\left\langle (1+\eta C) S_f \frac{\partial h_f}{\partial t} + \theta\eta \frac{\partial C}{\partial t}, \phi^{h_f} \right\rangle = &- \left\langle (1+\eta C)\mathbf{K_f} \left(\nabla h_f + \eta C \nabla z\right), \nabla \phi^{h_f} \right\rangle \\ &+ \left\langle \frac{\rho_R}{\rho_f} Q_R - (1+\eta C) Q_P, \phi^{h_f} \right\rangle \\ &+ \left\langle \left((1+\eta C)\mathbf{K_f} \left(\nabla h_f + \eta C \nabla z\right)\right) \cdot \mathbf{n}, \phi^{h_f} \right\rangle_{\Gamma_N^h}\end{aligned} \tag{3.1}$$

$$\begin{aligned}\left\langle \frac{\partial C}{\partial t}, \phi^C \right\rangle = &- \left\langle \mathbf{D}\nabla C, \nabla \phi^C \right\rangle + \left\langle \nabla C \cdot \frac{\mathbf{K}_f}{\theta} \left(\nabla h_f + \eta C \nabla z\right), \phi^C \right\rangle \\ &+ \left\langle \frac{C_R}{\theta} Q_R - \frac{C}{\theta} Q_P, \phi^C \right\rangle + \left\langle \mathbf{D}\nabla C \cdot \mathbf{n}, \phi^C \right\rangle_{\Gamma_N^C}\end{aligned} \tag{3.2}$$

To simplify the notation, the following expressions are used instead of the equations (3.1) and (3.2), respectively:

$$\left\langle (1+\eta C) S_f \frac{\partial h_f}{\partial t} + \theta\eta \frac{\partial C}{\partial t}, \phi^{h_f} \right\rangle = \mathcal{B}_F(h_f, C; \phi^{h_f}) + \mathcal{L}_F(\phi^{h_f}) \tag{3.3}$$

and

$$\left\langle \frac{\partial C}{\partial t}, \phi^C \right\rangle = \mathcal{B}_T(h_f, C; \phi^C) + \mathcal{L}_T(\phi^C) \tag{3.4}$$

3.1.1 Combination of Flow and Solute Transport Equations

The combined weak formulation of VDFST equations is derived as follows:
Let $V = H^1(\Omega) \times H^1(\Omega)$, and $V_0 = V_0^{h_f} \times V_0^C$. For $u(\mathbf{x}, t) = (h_f(\mathbf{x}, t), C(\mathbf{x}, t)) \in V$ for fixed t and $\phi = (\phi^{h_f}, \phi^C) \in V_0$ we define,

$$\begin{aligned} \mathcal{B}(u; \phi) &= \mathcal{B}_F(u, \phi^{h_f}) + \mathcal{B}_T(u, \phi^C) \\ \mathcal{L}(\phi) &= \mathcal{L}_F(\phi^{h_f}) + \mathcal{L}_T(\phi^C) \\ \mathcal{S}\left(\frac{\partial u}{\partial t}, \phi\right) &= \left\langle (1 + \eta C) S_f \frac{\partial h_f}{\partial t} + \theta\eta \frac{\partial C}{\partial t}, \phi^{h_f} \right\rangle + \left\langle \frac{\partial C}{\partial t}, \phi^C \right\rangle \end{aligned} \tag{3.5}$$

using the equations (3.3) and (3.4). Now the problem is finding $u(\mathbf{x}, t) = (h_f(\mathbf{x}, t), C(\mathbf{x}, t)) \in C^1([0, T], V)$ such that:

$$\begin{aligned} &\mathcal{S}\left(\frac{\partial u}{\partial t}, \phi\right) = \mathcal{B}(u; \phi) + \mathcal{L}(\phi) \;\; \forall \phi \in V_0, \; 0 \le t \le T \\ &h_f|_{\Gamma_D^{h_f}} = g_D^{h_f}, \;\; C|_{\Gamma_C^{h_f}} = g_D^C \\ &h_f(\mathbf{x}, 0) = h_f^0(\mathbf{x}), \;\; C(\mathbf{x}, 0) = C^0(\mathbf{x}) \end{aligned} \tag{3.6}$$

3.1.2 Finite Element Discretization with GFEM

Now, the infinite dimensional variational problem can be approximated by the Galerkin finite element method. The approximate solutions of freshwater hydraulic head and solute concentration can be written as the linear combination of time coefficients and nodal basis vectors [36, 37]:

$$
\begin{aligned}
h_f(\mathbf{x},t) &= \hat{h}(\mathbf{x},t) = \sum_{i=1}^{N} h_i(t)\phi_i(\mathbf{x}) \\
C(\mathbf{x},t) &= \hat{C}(\mathbf{x},t) = \sum_{i=1}^{N} C_i(t)\phi_i(\mathbf{x})
\end{aligned}
\tag{3.7}
$$

where $h_i(t)$ and $C_i(t)$ are the time coefficients at node i ($i = 1, ..., N$) and time t for the freshwater hydraulic head and solute concentration, respectively. $\phi_i(\mathbf{x})$ is the finite-element basis function at node i, and N is the number of the nodes across the domain. Replacing the freshwater hydraulic head h_f and concentration C by their approximations in the equation (3.6), the problem can be described as:

Find $\hat{u}(\mathbf{x},t) = (\hat{h}(\mathbf{x},t), \hat{C}(\mathbf{x},t)) \in C^1([0,T], \hat{V})$ where $\hat{V} \subset V$ such that

$$
\begin{aligned}
&\mathcal{S}\left(\frac{\partial \hat{u}}{\partial t}, \hat{\phi}_i\right) = \mathcal{B}(\hat{u}; \hat{\phi}_i) + \mathcal{L}(\hat{\phi}_i), \quad \forall \hat{\phi}_i \in \hat{V}_0,\ 0 \le t \le T \\
&\hat{h}|_{\Gamma_D^h} = \hat{g}_D^h,\ \ \hat{C}|_{\Gamma_D^C} = \hat{g}_D^C \\
&\hat{h}(\mathbf{x},0) = \hat{h}^0(\mathbf{x}),\ \ \hat{C}(\mathbf{x},0) = \hat{C}^0(\mathbf{x})
\end{aligned}
\tag{3.8}
$$

Let $\mathbf{u}(t)$ be the finite element expansion coefficients of $\hat{u}$. Then the Galerkin problem can be written as a nonlinear system of ordinary differential equations as:

$$
\begin{aligned}
M\dot{\mathbf{u}} &= \mathbf{F}(\mathbf{u}) + \mathbf{b},\ \ 0 \le t \le T \\
\mathbf{u}(0) &= \mathbf{u}_0
\end{aligned}
\tag{3.9}
$$

To integrate the equation system (3.9) in time, an implicit time-extrapolated method was used, and the boundary conditions were implemented into the global matrices. The system was solved using the Newton iteration approach, and the element integrals in all problems were approximated using Gaussian quadrature. Since the global matrices in the equation system depend on the number of nodes, the procedure may lead to large amount of calculation effort. These procedures are computationally expensive, but the application of the POD model significantly reduces the computation time.

Chapter 4

PROPER ORTHOGONAL DECOMPOSITION FOR VDFST

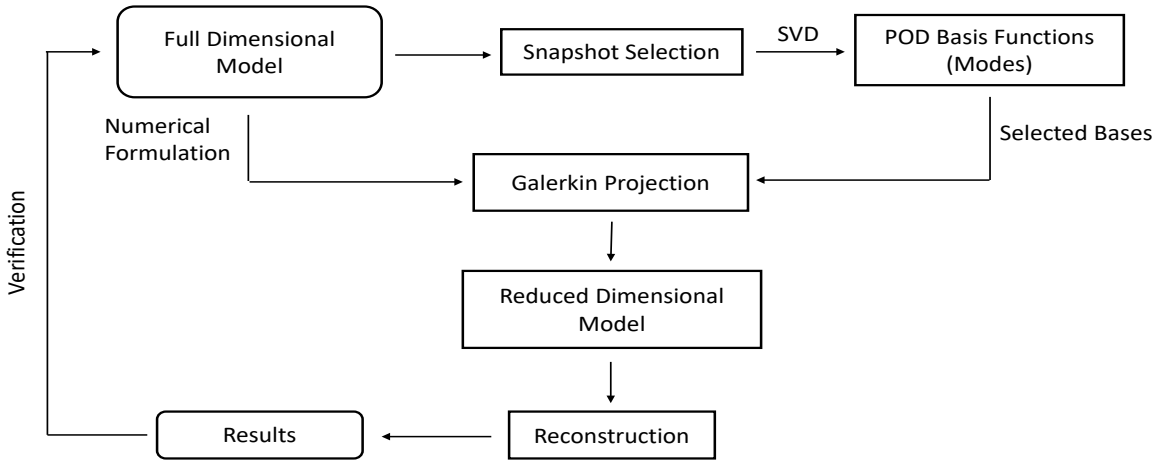

Figure 4.1 Reduced Order Modeling Methodology

POD is an efficient model order reduction technique to extract low dimensional basis functions from an ensemble of experimental or detailed simulation data of high dimensional systems. POD provides efficient tools to derive surrogate models for high-dimensional dynamical systems and partial differential equations when it is used in conjunction with Galerkin projection. The reason is that when the dynamical system and PDEs are projected onto a subspace of the original phase space, in combination with Galerkin projection, the subspace inherits special characteristics of overall solutions. Although POD is applied to nonlinear problems, it requires only standard matrix calculations which is a big advantage to reduce the computational cost.

The methodology of the reduced dimensional model that is given in the Figure 4.1 is modified from Li et al. [36, 37]. Firstly, the original full dimensional model is run, and an ensemble of time snapshots containing the spatial distribution of the numerical simulation at certain time instances reflecting the system dynamics is generated. The choice of the snapshots plays a crucial role and relies either on guesswork, intuition or simulations. Secondly, these snapshots are written as the columns of a matrix, and then POD bases are extracted applying SVD. The chosen bases are used with Galerkin projection to generate the reduced dimensional system. For the VDFST system, the variables of the reduced dimensional system are the time coefficients of the freshwater hydraulic head and the solute concentration. Finally, these time coefficients are used to reconstruct model states.

4.1 Snapshot Selection

Snapshots are constructed from the trajectories of the dynamical system and defined as a full spatial representation of the system state at certain instances of time. The performance of a reduced dimensional model which is constructed by a projection based method is highly sensitive to the selected snapshot set. To get more accurate results, snapshots should be chosen whenever the dynamics of the system change. For the VDFST model, the freshwater hydraulic head and solute concentration are the most important data resulting from numerical simulation and can be written as:

$$h_f^k = \begin{bmatrix} h_{f,1}^k \\ h_{f,2}^k \\ \vdots \\ h_{f,N}^k \end{bmatrix} \in \mathbb{R}^N \quad \text{and} \quad C^k = \begin{bmatrix} C_1^k \\ C_2^k \\ \vdots \\ C_N^k \end{bmatrix} \in \mathbb{R}^N$$

where N is the number of nodes across the mesh.

An ensemble of snapshots chosen in the time interval $[0, T]$ can be written as the columns of the following rectangular matrices for the freshwater hydraulic head and solute concentration respectively as $W_{h_f} = [h_f^1 \quad h_f^2 \quad \dots \quad h_f^{n_s}] \in \mathbb{R}^{N \times n_s}$ and $W_C = [C^1 \quad C^2 \quad \dots \quad C^{n_s}] \in \mathbb{R}^{N \times n_s}$ where N is the number of nodes across the mesh, and n_s is the number of the snapshots.

4.2 SVD and Construction of the POD Basis

Singular value decomposition (SVD) is a well-known method to extract POD basis. SVD of a matrix $W \in \mathbb{R}^{N \times n_s}$ with rank d is the factorization of W into the product of three matrices such that $W = U\Sigma V^T$ where the columns of $U \in \mathbb{R}^{N \times N}$ and $V \in \mathbb{R}^{n_s \times n_s}$ are orthonormal. The matrix $\Sigma \in \mathbb{R}^{N \times n_s}$ is diagonal with positive real entries such that [44]:

$$U^T W V = \begin{pmatrix} \Sigma_d & 0 \\ 0 & 0 \end{pmatrix} = \Sigma \in \mathbb{R}^{N \times ns}$$

where $\Sigma_d = \text{diag}(\sigma_1, ..., \sigma_d) \in \mathbb{R}^{d \times d}$. The positive numbers σ_i are called singular values of W and arranged in descending order. The columns of $U = (u_1, ..., u_N)$ and $V = (v_1, ..., v_{n_s})$ are called left singular vectors and right singular vectors respectively and satisfy the equations $Wv_i = \sigma_i u_i$ and $W^T u_i = \sigma_i v_i$ where $i = 1, ..., d$.

Using the Lagrangian formalism, it can be seen that columns of U and V also satisfy the following eigenvalue problems respectively:

$WW^T u = \sigma^2 u$ and $W^T W v = \sigma^2 v$ where $WW^T \in \mathbb{R}^{N \times N}$ and $W^T W \in \mathbb{R}^{n_s \times n_s}$. The singular values σ are square roots of the eigenvalues from WW^T or $W^T W$. It is clear that the eigenvalues of WW^T or $W^T W$ are indeed the same.

The relation between POD and SVD lies in the fact that the POD basis should contain as much "information" or "energy" as possible, and it can be seen that for every $d \leq n_s$ the approximation of the columns $W \in \mathbb{R}^{N \times n_s}$ by the first d singular vectors $\{u_1, ..., u_d\}$ is optimal in the least quares sense among all rank approximations to the columns of W.

In fluid dynamics, it is usually observed that the eigenvalues decrease exponentially. Using the corresponding eigenvectors of $W^T W$ as POD basis for the largest eigenvalues gives a good chance to derive low-order approximate models with a lower computational burden. Applying SVD to the matrices W_{h_f} and W_C with this idea yields the following POD basis functions which are optimally approximating the given data set in the least-squares sense for the freshwater hydraulic head and solute concentration:

$\Psi^{h_f} = \{\psi^{h_f,1}, \psi^{h_f,2}, ..., \psi^{h_f,M_{h_f}}\}$ and $\Psi^C = \{\psi^{C,1}, \psi^{C,2}, ..., \psi^{C,M_C}\}$ where M_{h_f} and M_C are

the number of the POD bases from the snapshots of the freshwater hydraulic head and solute concentration respectively.

4.3 Galerkin Projection and POD

To generate the reduced dimensional model, we obtain an ensemble of the snapshots solving the full dimensional model (3.8), and then we derive the POD bases using SVD. Since the goal is to project the full dimensional model onto a reduced dimensional subspace that is spanned by the POD modes, Galerkin method is used. It is a key step in this process and helps to smooth the derivatives of the POD basis functions.

The model variables h_f and C can be expressed as a linear combination of the GFEM basis functions, POD modes and time coefficients as [36, 37]:

$$\begin{cases} h_f(\mathbf{x},t) \approx \tilde{h}_f(\mathbf{x},t) = \sum_{i=1}^{M_{h_f}} \sum_{j=1}^{N} \phi_j(\mathbf{x}) \psi_j^{h_f,i} a_i^{h_f}(t) \\ C(\mathbf{x},t) \approx \tilde{C}(\mathbf{x},t) = \sum_{i=1}^{M_C} \sum_{j=1}^{N} \phi_j(\mathbf{x}) \psi_j^{C,i} a_i^{C}(t) \end{cases} \tag{4.1}$$

Using the equations (2.29) and (2.30), the following residual functions are defined:

$$\mathcal{R}_F = \nabla \cdot \Big((1+\eta C)\mathbf{K_f} \big[\nabla h_f + \eta C \nabla z \big] \Big) - (1+\eta C) S_f \frac{\partial h_f}{\partial t} - \theta \eta \frac{\partial C}{\partial t} + \frac{\rho_R}{\rho_f} Q_R - (1+\eta C) Q_P \tag{4.2}$$

$$\mathcal{R}_T = \quad \nabla \cdot (\mathbf{D} \nabla C) + \nabla C \cdot \frac{\mathbf{K}_f}{\theta} \left(\nabla h_f + \eta C \nabla z \right) - \frac{\partial C}{\partial t} + \frac{C_R}{\theta} Q_R - \frac{C}{\theta} Q_P \tag{4.3}$$

An ordinary differential equation system governing the time coefficients $a^{h_f}(t)$ and $a^C(t)$ is obtained by substituting (4.1) into the residual equations (4.2) and (4.3) projecting onto the subspace spanned by the modes $\psi^{h_f,m}$ and $\psi^{C,m}$ as follows [36, 37]:

$$\begin{aligned} \Big\langle \big\langle \mathcal{R}_F(\tilde{h}_f, \tilde{C}, \mathbf{x}, t), \phi_k \big\rangle, \psi^{h_f,m} \Big\rangle = 0 \quad k = 1, ..., N; \quad m = 1, ..., M_{h_f} \\ \Big\langle \big\langle \mathcal{R}_T(\tilde{C}, \tilde{h}_f, \mathbf{x}, t), \phi_k \big\rangle, \psi^{C,m} \Big\rangle = 0 \quad k = 1, ..., N; \quad m = 1, ..., M_C \end{aligned} \tag{4.4}$$

where M_{h_f} and M_C are the number of modes for freshwater hydraulic head and solute concentration respectively. Expanding the equation system (4.4), the following reduced dimensional

model can be derived:

$$\left\langle \iint_{\Omega} \begin{bmatrix} \nabla \cdot \Big((1+\eta\tilde{C})\mathbf{K_f}\big[\nabla\tilde{h}_f + \eta\tilde{C}\nabla z\big]\Big) - (1+\eta\tilde{C})S_f\frac{\partial\tilde{h}_f}{\partial t} \\ -\theta\eta\frac{\partial\tilde{C}}{\partial t} + \frac{\rho_R}{\rho_f}Q_R - (1+\eta\tilde{C})Q_P \end{bmatrix} \psi_k \, d\Omega, \Psi^{h_f} \right\rangle = 0 \qquad (4.5)$$

$$\left\langle \iint_{\Omega} \begin{bmatrix} \nabla \cdot \Big(\mathbf{D}\nabla\tilde{C}\Big) + \nabla\tilde{C} \cdot \frac{\mathbf{K}_f}{\theta}\Big(\nabla\tilde{h}_f + \eta\tilde{C}\nabla z\Big) \\ -\frac{\partial\tilde{C}}{\partial t} + \frac{C_R}{\theta}Q_R - \frac{\tilde{C}}{\theta}Q_P \end{bmatrix} \psi_k \, d\Omega, \Psi^{C} \right\rangle = 0 \qquad (4.6)$$

It is usually acceptable that the principal axes are horizontal and vertical for an aquifer with horizontal bedding. Thus, according to the assumption the variables $\tilde{h}_f$, $\tilde{C}$, the tensors $\mathbf{K_f}$, $\mathbf{D}$ and the vector ∇z can written respectively as $\tilde{h}_f(\mathbf{x},t) = \tilde{h}_f(x,z,t)$, $\tilde{C}(\mathbf{x},t) = \tilde{C}(x,z,t)$, $\mathbf{K_f} = \begin{bmatrix} K_{fx} & 0 \\ 0 & K_{fz} \end{bmatrix}$, $\mathbf{D} = \begin{bmatrix} D_{xx} & 0 \\ 0 & D_{zz} \end{bmatrix}$, $\nabla z = \begin{bmatrix} 0 \\ 1 \end{bmatrix}$.

Letting $\mathcal{T}_\Delta$ be a triangulation of $\Omega \in \mathbb{R}^2$ consisting of a collection of N_e elements, $\{\Omega_e\}_{e=1}^{N_e}$, the following semi-discrete coupled ODE system can be stated as follows [36, 37]:

$$\begin{aligned} A_1 a^{h_f} + (a^C)^T A_2 a^{h_f} + A_3 a^C + (a^C)^T A_4 a^C + A_5\frac{da^{h_f}}{dt} + (a^C)^T A_6\frac{da^{h_f}}{dt} + A_7\frac{da^C}{dt} &= F_1 \\ B_1 a^C - (a^{h_f})^T B_2 a^C - (a^C)^T B_3 a^C + B_4\frac{da^C}{dt} &= F_2 \end{aligned} \qquad (4.7)$$

with the following initial conditions:

$a_m^{h_f}(t_0) = \big\langle h_f(x,z,t_0), \psi^{h_f,m}\big\rangle, \quad m = 1, ..., m_{h_f}$

$a_m^{C}(t_0) = \big\langle C(x,z,t_0), \psi^{C,m}\big\rangle, \quad m = 1, ..., m_{C}$

where

$$a^{h_f}(t) = \begin{bmatrix} a_{1_{h_f}}(t) \\ a_{2_{h_f}}(t) \\ \vdots \\ a_{m_{h_f}}(t) \end{bmatrix} \quad \text{and} \quad a^{C}(t) = \begin{bmatrix} a_{1_{C}}(t) \\ a_{2_{C}}(t) \\ \vdots \\ a_{m_{C}}(t) \end{bmatrix}$$

The matrices $A_1 - A_7$, $B_1 - B_4$, F_1 and F_2 can be shown to be:

$$A_1 = (\Psi^{h_f})^T \alpha_1 \Psi^{h_f}; \quad \alpha_{1i,j} = \sum_e \left\{ \iint_e \left[K_{fx}^e \frac{\partial\phi_i}{\partial x}\frac{\partial\phi_j}{\partial x} + K_{fz}^e \frac{\partial\phi_i}{\partial z}\frac{\partial\phi_j}{\partial z} \right] dxdz \right\}$$

$$A_2 = (\Psi^{h_f})^T \alpha_2 \Psi^{h_f}; \quad \alpha_{2i,j,m} = \sum_{m=1}^{M_C} \sum_e \left\{ \iint_e \eta \sum_{j=1}^{3} \phi_j \psi_j^{C,m} \begin{bmatrix} K_{fx}^e \frac{\partial \phi_i}{\partial x} \frac{\partial \phi_j}{\partial x} \\ +K_{fz}^e \frac{\partial \phi_i}{\partial z} \frac{\partial \phi_j}{\partial z} \end{bmatrix} dxdz \right\}$$

$$A_3 = (\Psi^{h_f})^T \alpha_3 \Psi^{C}; \quad \alpha_{3i,j} = \sum_e \left\{ \iint_e \left[\eta K_{fz}^e \frac{\partial \phi_i}{\partial z} \phi_j - \eta Q_P \phi_i \phi_j \right] dxdz \right\}$$

$$A_4 = (\Psi^{h_f})^T \alpha_4 \Psi^{C}; \quad \alpha_{4i,j,m} = \sum_{m=1}^{M_C} \sum_e \left\{ \iint_e \eta^2 K_{fz}^e \sum_{j=1}^{3} \phi_j \psi_j^{C,m} \frac{\partial \phi_i}{\partial z} \phi_j \, dxdz \right\}$$

$$A_5 = (\Psi^{h_f})^T \alpha_5 \Psi^{h_f}; \quad \alpha_{5i,j} = \sum_e \left\{ \iint_e S_f \phi_i \phi_j \, dxdz \right\}$$

$$A_6 = (\Psi^{h_f})^T \alpha_6 \Psi^{h_f}; \quad \alpha_{6i,j,m} = \sum_{m=1}^{M_C} \sum_e \left\{ \iint_e S_f \eta \sum_{j=1}^{3} \phi_j \psi_j^{C,m} \phi_i \phi_j \, dxdz \right\}$$

$$A_7 = (\Psi^{h_f})^T \alpha_7 \Psi^{C}; \quad \alpha_{7i,j} = \sum_e \left\{ \iint_e \theta \eta \phi_i \phi_j \, dxdz \right\}$$

$$F_1 = (\Psi^{h_f})^T \sum_e \left\{ \int_{\Gamma_2} \frac{\rho_q}{\rho_f} q \phi_i \, d\Gamma + \iint_e Q_P \phi_i \, dxdz - \iint_e \frac{\rho_R}{\rho_f} Q_R \phi_i \, dxdz \right\}$$

$$B_1 = (\Psi^{C})^T \beta_1 \Psi^{C}; \quad \beta_{1i,j} = \sum_e \left\{ \iint_e \left[D_{xx}^e \frac{\partial \phi_i}{\partial x} \frac{\partial \phi_j}{\partial x} + D_{zz}^e \frac{\partial \phi_i}{\partial z} \frac{\partial \phi_j}{\partial z} + \frac{q_{ss}}{\theta} \phi_i \phi_j \right] dxdz \right\}$$

$$B_2 = (\Psi^{C})^T \beta_2 \Psi^{C}; \quad \beta_{2i,j,m} = \sum_{m=1}^{M_{h_f}} \sum_e \left\{ \iint_e \begin{bmatrix} \frac{K_{fx}^e}{\theta} \sum_{j=1}^{3} \frac{\partial \phi_j}{\partial x} \psi_j^{h_f,m} \cdot \phi_i \frac{\partial \phi_j}{\partial x} \\ +\frac{K_{fz}^e}{\theta} \sum_{j=1}^{3} \frac{\partial \phi_j}{\partial z} \psi_j^{h_f,m} \cdot \phi_i \frac{\partial \phi_j}{\partial z} \end{bmatrix} dxdz \right\}$$

$$B_3 = (\Psi^{C})^T \beta_3 \Psi^{C}; \quad \beta_{3i,j,m} = \sum_{m=1}^{M_C} \sum_e \left\{ \iint_e \frac{\eta K_{fz}^e}{\theta} \sum_{j=1}^{3} \phi_j \psi_j^{C,m} \cdot \phi_i \frac{\partial \phi_j}{\partial z} \, dxdz \right\}$$

$$B_4 = (\Psi^{C})^T \beta_4 \Psi^{C}; \quad \beta_{4i,j} = \sum_e \left\{ \iint_e \phi_i \phi_j \, dxdz \right\}$$

$$F_2 = (\Psi^{C})^T \sum_e \left\{ \int_{\Gamma_2} g \phi_i \, d\Gamma + \iint_e \frac{q_{ss}}{\theta} C_{ss} \phi_i \, dxdz \right\}$$

where $i = 1, ..., N \quad j = 1, ..., N$.

Since the dimensions of $\Psi^{h_f} \in \mathbb{R}^{N \times nb}$ and $\Psi^{C} \in \mathbb{R}^{N \times nb}$ depend on the number of POD bases, the dimension of the reduced-order model (4.7) is much smaller than the dimension of the full dimensional system (3.9). Thus, solving the equation system (4.7) saves a large amount computational labor with an acceptable error.

4.4 Solution Method with Newton Iteration

In [36, 37], the full dimensional and reduced dimensional VDFST models were solved using coupling iteration scheme. Since the Newton iteration is usually faster, we used this iteration scheme for both the full dimensional and reduced dimensional models. To test our solution technique, we used the Henry and Elder problems. The coupling and Newton iteration methods were compared. In many cases for reproduction and prediction calculations, the Newton iteration converged faster than the coupling iteration. To solve the reduced order model, first, we define the following discrete weak residuals:

$$\begin{aligned}\tilde{\mathcal{R}}_F^k =& A_1 a^{h_f(n+1,k)} + (a^{C(n+1,k)})^T A_2 a^{h_f(n+1,k)} + A_3 a^{C(n+1,k)} \\ &+ (a^{C(n+1,k)})^T A_4 a^{C(n+1,k)} + A_5 \frac{a^{h_f(n+1,k)} - a^{h_f(n,0)}}{\Delta t} \\ &+ (a^{C(n+1,k)})^T A_6 \frac{a^{h_f(n+1,k)} - a^{h_f(n,0)}}{\Delta t} + A_7 \frac{a^{C(n+1,k)} - a^{C(n,0)}}{\Delta t} - F_1\end{aligned} \tag{4.8}$$

$$\begin{aligned}\tilde{\mathcal{R}}_T^k =& B_1 a^{C(n+1,k)} - (a^{h_f(n+1,k)})^T B_2 a^{C(n+1,k)} - (a^{C(n+1,k)})^T B_3 a^{C(n+1,k)} \\ &+ B_4 \frac{a^{C(n+1,k)} - a^{C(n,0)}}{\Delta t} - F_2\end{aligned} \tag{4.9}$$

where n is the current time step and $\Delta t = t^{n+1} - t^n$.

Letting $u^{n+1,k} = [a^{h_f(n+1,k)}(t), a^{C(n+1,k)}(t)]^T$, the system residual at the time step $n+1$ and the iteration k can be given by $\tilde{\mathcal{R}}^k(u^{n+1,k}) = [\tilde{\mathcal{R}}_F^k(u^{n+1,k}), \tilde{\mathcal{R}}_T^k(u^{n+1,k})]^T$.

Finally, defining our Newton iterate $\Delta u = u^{n+1,k+1} - u^{n+1,k}$, the solution algorithm for each time step can be written as:

1. Initialize iteration value: $u^{n+1,1} = u^n$

2. For $k = 1, 2, ...$ until convergence:

   (a) Compute residual $\tilde{\mathcal{R}}^k(u^{n+1,k}) = \begin{bmatrix} \tilde{\mathcal{R}}_F^k(u^{n+1,k}) \\ \tilde{\mathcal{R}}_T^k(u^{n+1,k}) \end{bmatrix}$

(b) Compute Jacobian $\tilde{\mathcal{J}}(u^{n+1,k}) = \begin{bmatrix} \frac{\partial \tilde{\mathcal{R}}_F^k}{\partial a^{h_f(n+1,k)}} & \frac{\partial \tilde{\mathcal{R}}_F^k}{\partial a^{C(n+1,k)}} \\ \frac{\partial \tilde{\mathcal{R}}_T^k}{\partial a^{h_f(n+1,k)}} & \frac{\partial \tilde{\mathcal{R}}_T^k}{\partial a^{C(n+1,k)}} \end{bmatrix}$

(c) Solve the linearized system for Δu:
$\tilde{\mathcal{J}}(u^{n+1,k})\Delta u = -\tilde{\mathcal{R}}^k(u^{n+1,k})$

(d) Update $u^{n+1,k+1} = \Delta u + u^{n+1,k}$.

(e) Test for convergence by testing $||a^{C(n+1,k+1)} - a^{C(n+1,k)}|| < \tau_s$ for some suitable error tolerances τ_s.

After calculating a^C and a^{h_f} for each time step, the variables $\tilde{C}$ and $\tilde{h}_f$ can be constructed using the equations (4.1).

Element integrals in all problems were approximated using Gaussian quadrature for both full dimensional and reduced dimensional models.

4.5 Error Analysis

Di et al. [16] provided some error estimates between the numerical solutions of the full dimensional model and the reduced dimensional model based on POD bases.

Let $C^n \in \mathbb{R}^N$ and $\tilde{C}^n \in \mathbb{R}^N$ be the vectors constituted with solutions of the original and reduced dimensional models for solute concentration respectively for the n_{th} $(n = 1, 2, ..., T)$ time step.

Let $W_C = [C^1 \quad C^2 \quad ... \quad C^{n_s}] \in \mathbb{R}^{N \times n_s}$ be an ensemble of snapshots for solute concentration where N is the number of nodes across the mesh, and n_s is the number of the snapshots. If n is chosen from the set $\{1, 2, ..., n_s\}$, the error estimate is obtained as follows [16]:

$||C^n - \tilde{C}^n||_{L_2} \leq \sqrt{\lambda_{M_C+1}} \quad n \in \{1, 2, ..., n_s\}$

where λ represents the eigenvalues of the matrices $W_C^T W_C$ or $W_C W_C^T$. M_C is the number of basis functions chosen for the reduced dimensional model.

Else if $n \notin \{1, 2, ..., n_s\}$, when t_ℓ $(1 \leq \ell \leq n_s)$ are uniformly chosen from t_n $(1 \leq \ell \leq T)$, and $\left\| \frac{\partial C(\zeta_1)}{\partial t} \right\|_{L_2}$ and $\left\| \frac{\partial \tilde{C}(\zeta_2)}{\partial t} \right\|_{L_2}$ are bounded (i.e. $\left\| \frac{\partial C(\zeta_1)}{\partial t} \right\|_{L_2} \leq \omega$ and $\left\| \frac{\partial \tilde{C}(\zeta_2)}{\partial t} \right\|_{L_2} \leq \omega$), the following error estimate exists [16]:

$||C^n - \tilde{C}^n||_{L_2} \leq \sqrt{\lambda_{M_C+1}} + \frac{\Delta tT}{2n_s}\omega \quad n \notin \{1, 2, ..., n_s\}$

where $t_n \leq \zeta_1 \leq t_\ell$ and $t_n \leq \zeta_2 \leq t_\ell$.

Using the same method, some error estimates between the numerical solutions of the full dimensional model and the reduced dimensional model for freshwater hydraulic conductivity based on POD bases can be provided.

Chapter 5

NUMERICAL EXPERIMENTS: HENRY PROBLEM AND ELDER PROBLEM AS BENCHMARKS

5.1 The Henry Problem

The Henry salt water intrusion problem [24] has been used for decades as a test case for benchmarking density-dependent flow and solute transport models. Many numerical codes, such as SEAWAT and MODFLOW, have been evaluated with the Henry's semi-analytical results [24]. The original problem concerns a vertical cross-section through a confined aquifer that is isotropic and homogeneous. The conceptual design of the Henry problem is shown in Figure 5.1 [23]. The confined aquifer box is 2 meter long, 1 meter wide and 1 meter high. No flow conditions were specified along the lower and upper boundaries. A hydrostatic pressure distribution was specified for the seaside boundary (right side), and a freshwater flux was prescribed along the inland boundary from the regional aquifer system. Freshwater enters into the confined aquifer box from the left side at a constant rate ($Q_{in} = 5.702$ m^3/d per meter) with a fixed concentration ($C_{in} = 0$) and mixes with the saline water from the right boundary. There is no other source for water entering the aquifer or leaving through a sink.

Li et al. [36, 37] wrote numerical programs to solve the VDFST models using the GFEM with the coupling iteration. To examine the accuracy of these numerical programs, a standard Henry problem [59] was simulated in the domain that was discretized using 861 nodes and 1600 uniformly aligned linear triangular elements with the diagonal pointing in the NE-SW direction, and the concentration solutions of the full dimensional system were compared with the semi-analytical results [59]. Both the position and shape of the isochlors matched very well [36, 37]. Also, to increase the relative importance of the density-dependent effects, Li [36, 37]

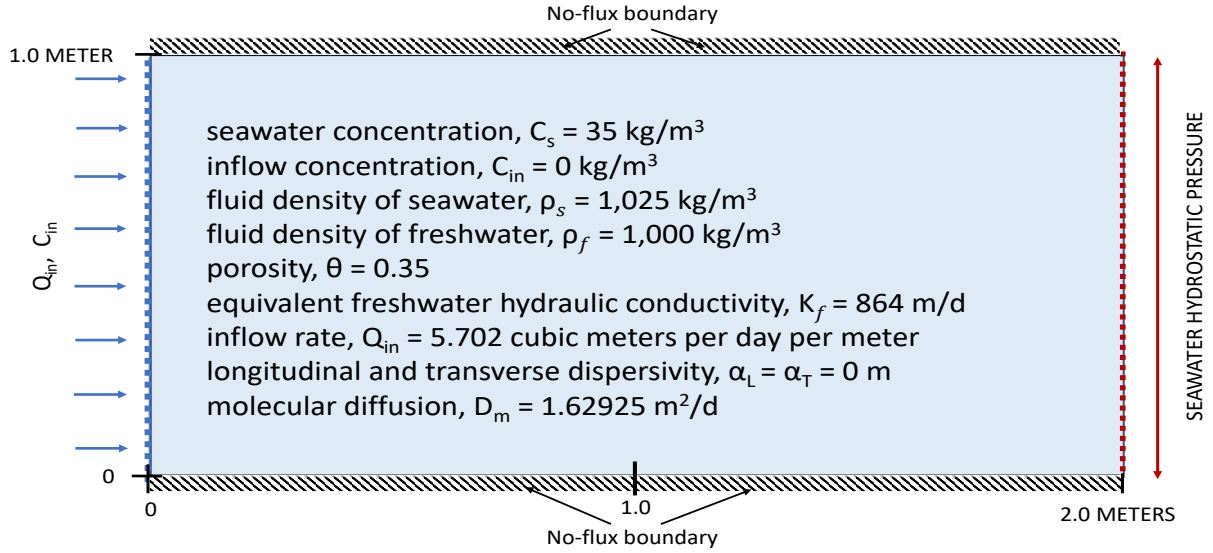

Figure 5.1 Model parameters for the standard Henry problem

simulated a modified Henry problem by just halving the recharge rate of freshwater (Q_{in}), and it was used as the original full model [59]. Both the standard and modified Henry problems were simulated using the same spatial and temporal discretization.

To solve and simulate the VDFST models, we ran the numerical programs using GFEM with Newton iteration. Both standard (Figure 5.2) and modified (Figure 5.3) Henry problems were simulated using the same model inputs as Li et al. [36, 37]. Also, the concentration and equivalent freshwater head solutions from these numerical models were compared with Li's solutions, and the isochlors matched excellently in Figure 5.4 and 5.5. The required CPU time to simulate 500 min in MATLAB with a time step of 1 min and a convergence criteria of 10^{-6} kg/m^3 for the fluid concentration between consecutive iterations is approximately 570 s for the modified full dimensional model using Newton iteration approach.

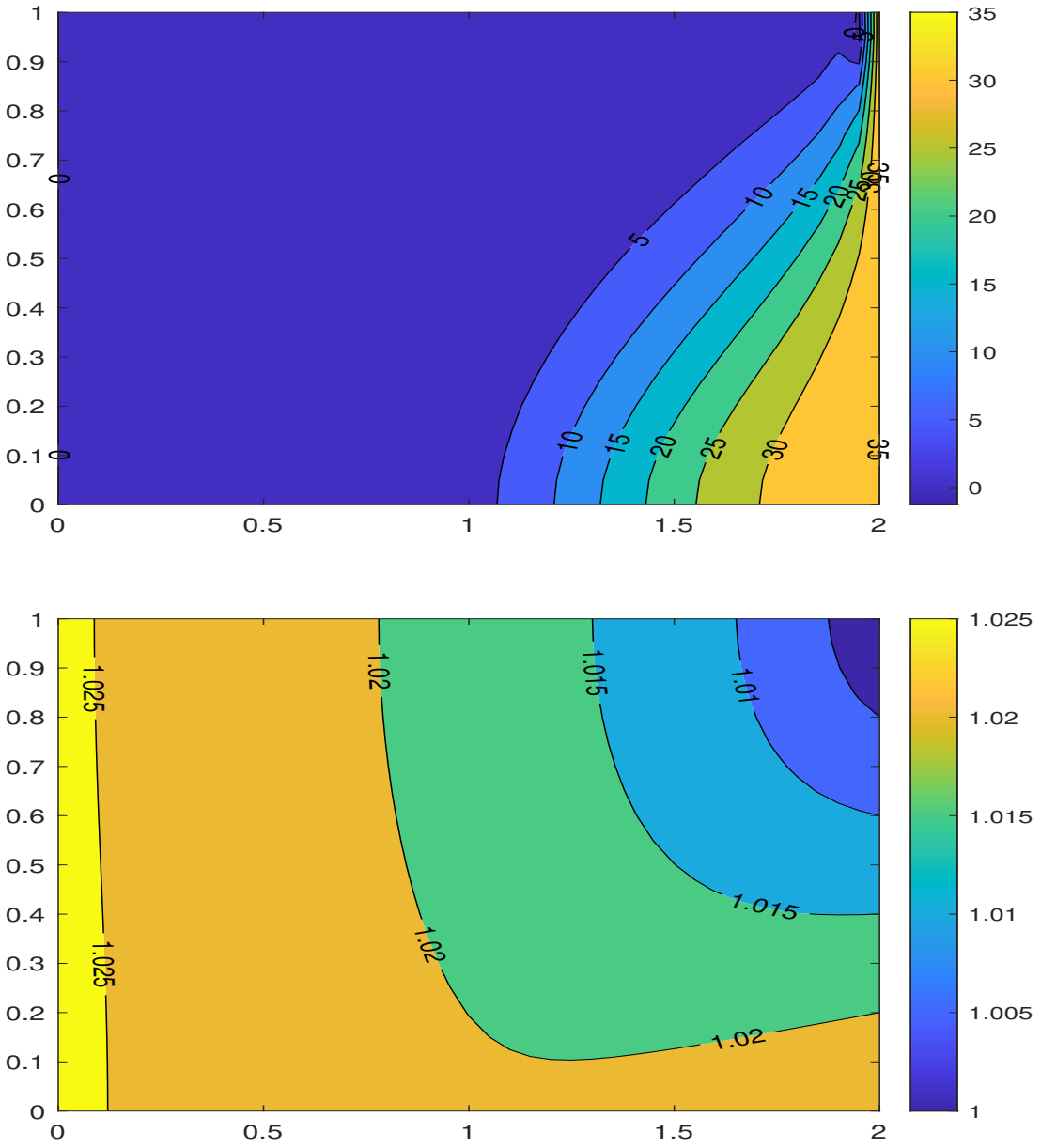

Figure 5.2 Numerical simulations of solute concentration (Top) and freshwater head (Bottom) at time t = 500 minutes for the standard Henry problem

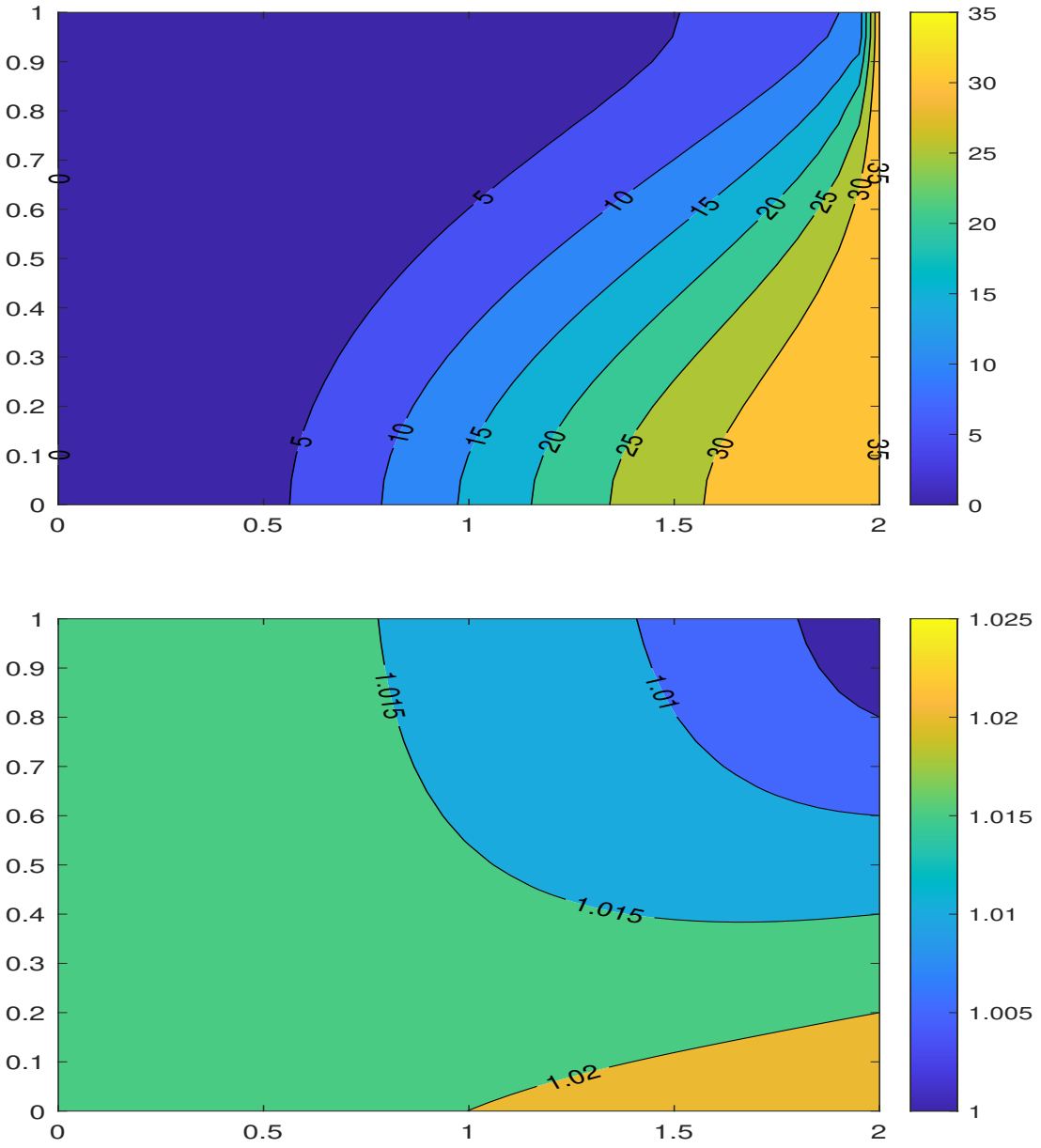

Figure 5.3 Numerical simulations of solute concentration (Top) and freshwater head (Bottom) at time t = 500 minutes for the modified Henry problem

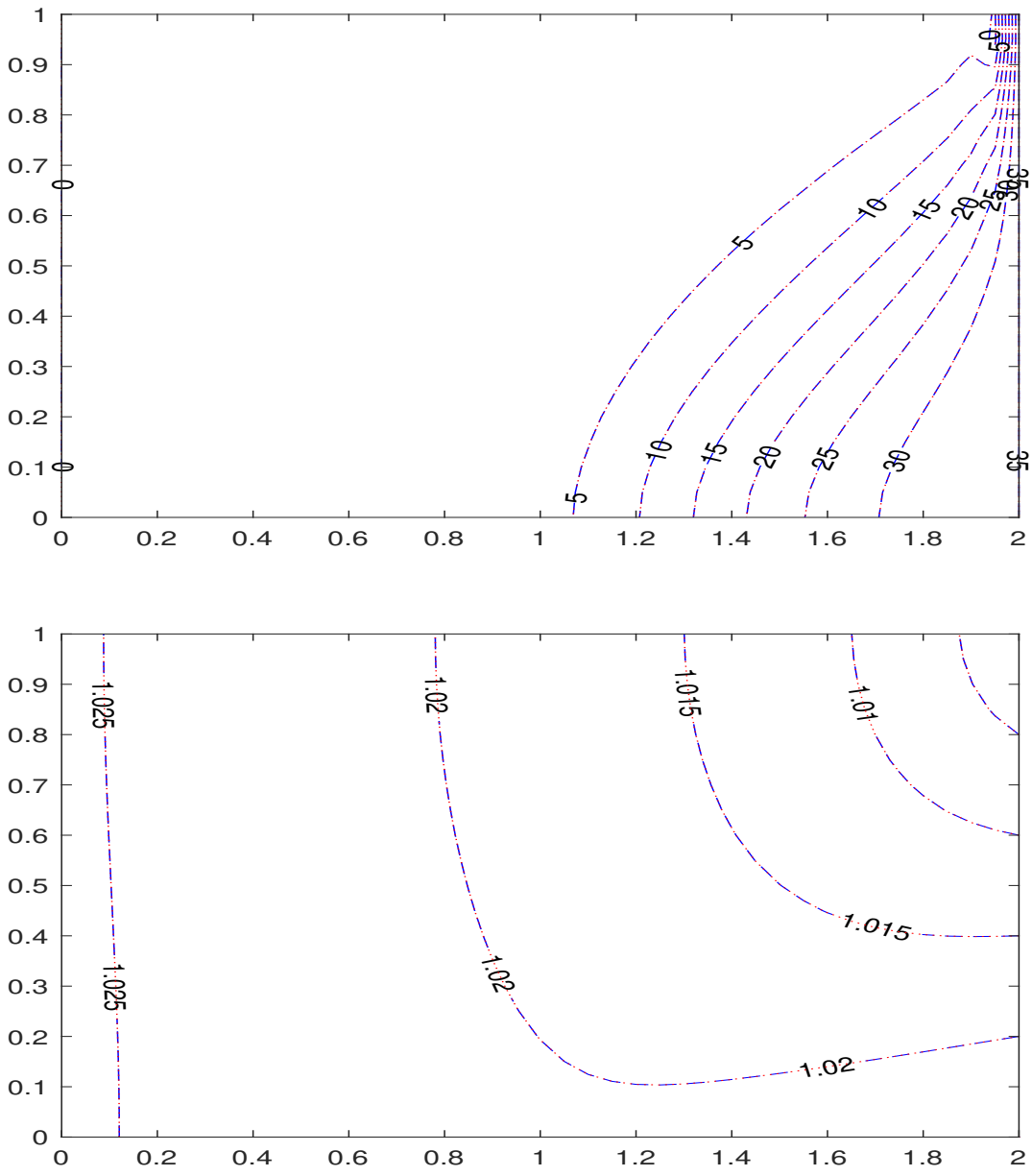

Figure 5.4 Comparison of the Newton (red dashed) and Coupling (blue dashed) iteration approaches for solute concentration (Top) and freshwater head (Bottom) at time t = 500 minutes for the standard Henry problem

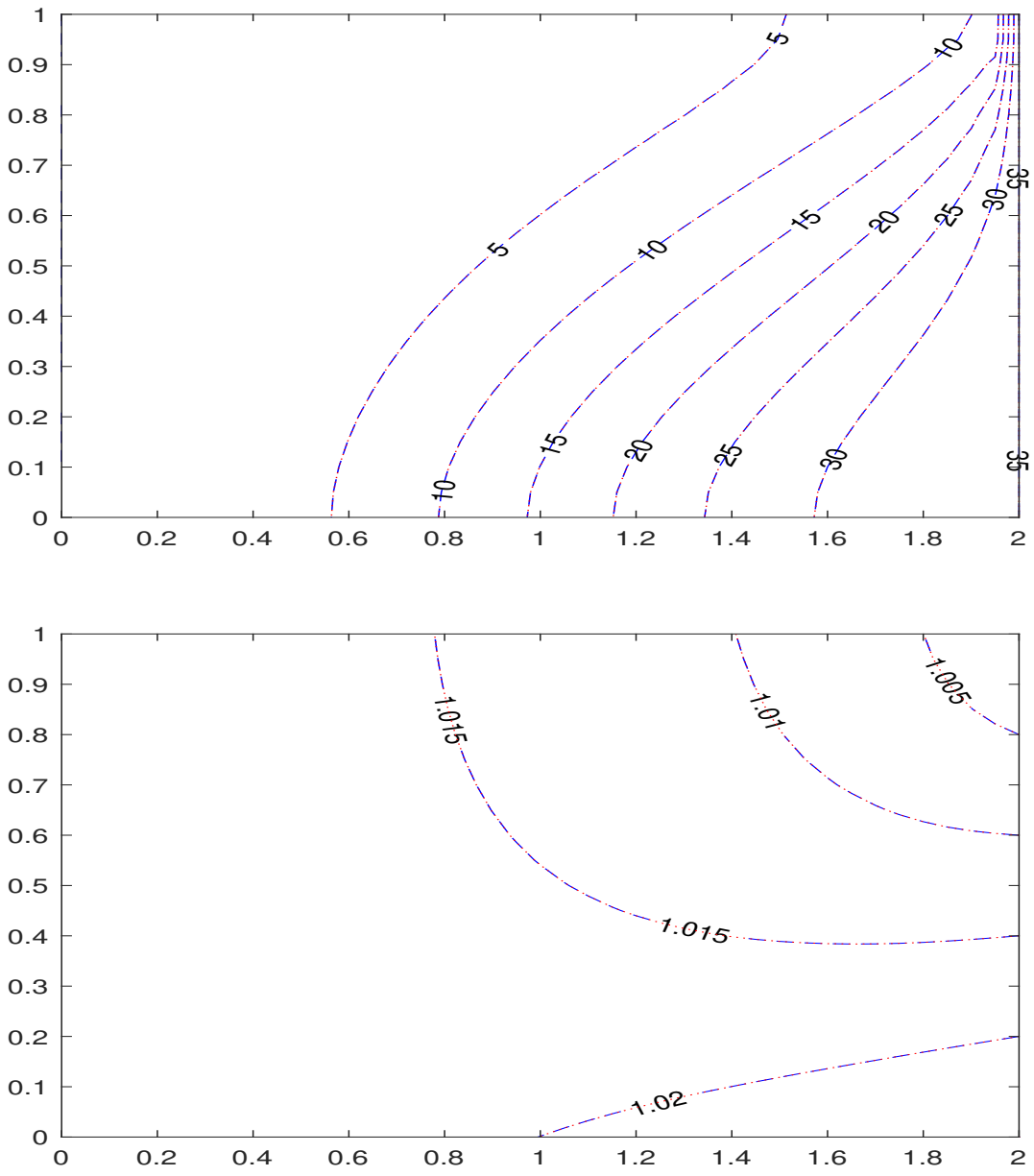

Figure 5.5 Comparison of the Newton (red dashed) and Coupling (blue dashed) iteration approaches for solute concentration (Top) and freshwater head (Bottom) at time t = 500 minutes for the modified Henry problem

5.2 Reduced Order Model of the Henry Problem

To test the capability of the model reduction method, modified Henry problem is used as the original problem under various cases. Modified Henry problem has several important advantages as compared to the standard solution in terms of the numerical methods because the reduced recharge can help alleviate problems with the oscillation in the solution of the advection-dispersion equation near the outflow boundary [59]. Also, the maximum grid Peclet number is reduced from Pe = 4.1 to Pe = 2.8 under the modified conditions with a uniform discretization ($\Delta x = \Delta z$ = 0.05 m) to avoid oscillatory solutions [68].

The predicted time length, number of the POD modes and snapshot selection are some of the important factors that affect the accuracy and efficiency of the reduced dimensional model on prediction. In the following subsections, the effects of these factors are illustrated with the comparison of the Newton and coupling iteration approaches.

Modified Henry Problem		
Number of Bases (nb)	Computation time (s) with Newton Iteration	Computation time (s) with Coupling Iteration
5	0.1408	0.2243
10	0.2664	0.4168
15	0.4292	0.6755
20	0.6381	0.9939
25	0.9109	1.3660
30	1.2461	1.9229

Table 5.1 Computation times (CPU) of the reduced dimensional model for the homogeneous case with different nb to simulate 500 time steps

5.2.1 Homogeneous Case

In this subsection, it is assumed that the hydraulic conductivity K_f is 864 m/day throughout a homogeneous and isotropic aquifer for both full and reduced dimensional models [23].

POD provides the most efficient way of capturing the dominant components of a high dimensional process with only an adequate number of modes. It means it is possible to reduce the model order from hundreds or thousands to a few tens with these modes. This reduction enables that such models can be applied in real time applications by resulting in ease of sim-

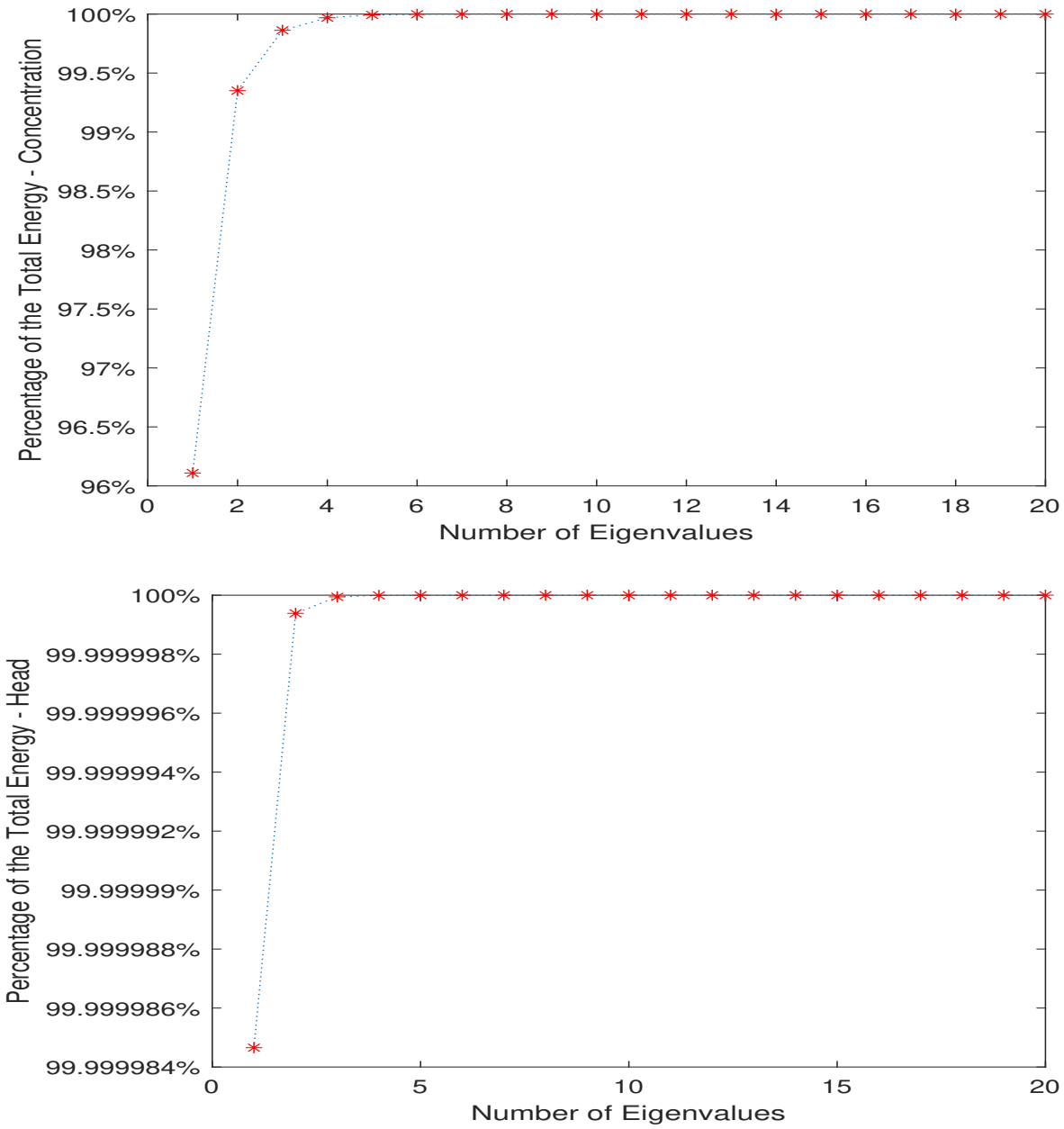

Figure 5.6 The percentages of the total energy of solute concentration (Top) and the total energy of the equivalent freshwater hydraulic head (Bottom) for the homogeneous case.

ulation, assimilation and optimization. In a dynamical system, large eigenvalues correspond to main characteristics of the system, while small eigenvalues give only small perturbations of the overall dynamics. The goal is to choose the number of POD modes small enough while the percentage of the total energy is close %100 [44]. The relation between the total energy and the number of the eigenvalues is shown in Figure 5.6 by choosing the snapshots every 1

minute from the full dimensional model solutions of the first 100 minutes for both freshwater hydraulic head and solute concentration.

The required CPU times to simulate 500 min in MATLAB with a time step of 1 min and a convergence criteria of 10^{-12} kg/m^3 for the time coefficients of fluid concentration, $a^C(t)$, between consecutive iterations are listed in Table 5.1 for the reduced dimensional model using Newton and coupling iteration approaches with different number of POD bases. The computation time using the full dimensional model to simulate 500 time steps is about 570 s. It took about 0.9109 s of CPU time with Newton iteration approach and 1.3660 s of CPU time with coupling iteration with 25 POD modes. Although it runs almost 415 times faster with coupling iteration, it runs at least 625 times faster with Newton iteration.

To compare the predicted results between the reduced and full dimensional models for each time step over the domain, root mean square error (RMSE) is used as an error metric:

$$E^i_{h_f} = \sqrt{\frac{(h^i_f - \tilde{h}^i_f)^T (h^i_f - \tilde{h}^i_f)}{N}} \qquad i \in \{1, 2, ..., T\} \tag{5.1}$$

and

$$E^i_C = \sqrt{\frac{(C^i - \tilde{C}^i)^T (C^i - \tilde{C}^i)}{N}} \qquad i \in \{1, 2, ..., T\} \tag{5.2}$$

where h_f and C are simulation results from full dimensional model, $\tilde{h}_f$ and $\tilde{C}$ are simulation results from reduced dimensional model, N is number of nodes throughout the domain and i $\in \{1, 2, ..., T\}$ is the i_{th} time step. In Figure 5.7, the RMSE of solute concentration between the reduced and full dimensional models increases as the number of prediction time steps increases. Also, it can be seen that accuracy increases as the number of POD basis functions increases, but after a certain basis size accuracy doesn't increase significantly. Thus, it is important to choose the optimal number of POD bases for the accuracy. In Figure 5.8, the predicted results using 25 bases is best at t=100 min. Although the accuracy is decreasing gradually from t=100 min to t =500 min, the isochlors of the reduced dimensional model and full dimensional model still match well at t=500 min. Figure 5.9 shows that both the Newton and coupled iteration time stepping approaches give the same RMSE over the simulation time interval, both for low and high dimensional POD subspaces.

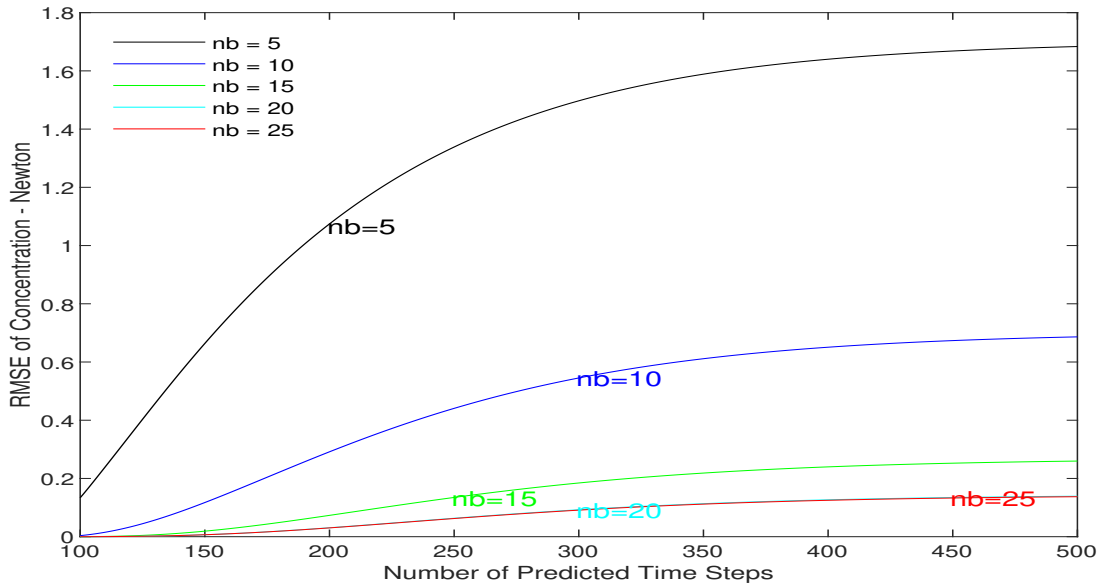

Figure 5.7 RMSE of predicted concentrations between the full dimensional and reduced dimensional models for the homogeneous case using Newton iteration with different number of bases

Snapshot selection is important to maximize the accuracy and efficiency of the reduced dimensional model. They should be chosen whenever the dynamics of the system change. If the addition of another snapshot doesn't contribute to accuracy significantly, it can be assumed that the number of snapshots is optimal. To investigate the effects of the number of snapshots, we sampled different number of snapshots from the first 100 minutes. 10, 25, 50 and 100 snapshots were taken with a sampling time step of 10 min, 4 min, 2 min and 1 min respectively with 25 POD bases, and the results are shown the Figure 5.10. It can be seen that the accuracy is increasing as the number of snapshots increases.

5.2.2 Heterogeneous Case

Hydraulic conductivity is a key parameter for all aspects of water and solute movement. Whether under saturated or unsaturated conditions, water movement is highly dependent on the hydraulic conductivity. To demonstrate the efficiency and accuracy of the model reduction technique (POD) with Newton iteration approach, it was tested in heterogeneous and anisotropic natural media conditions since it is more "realistic".

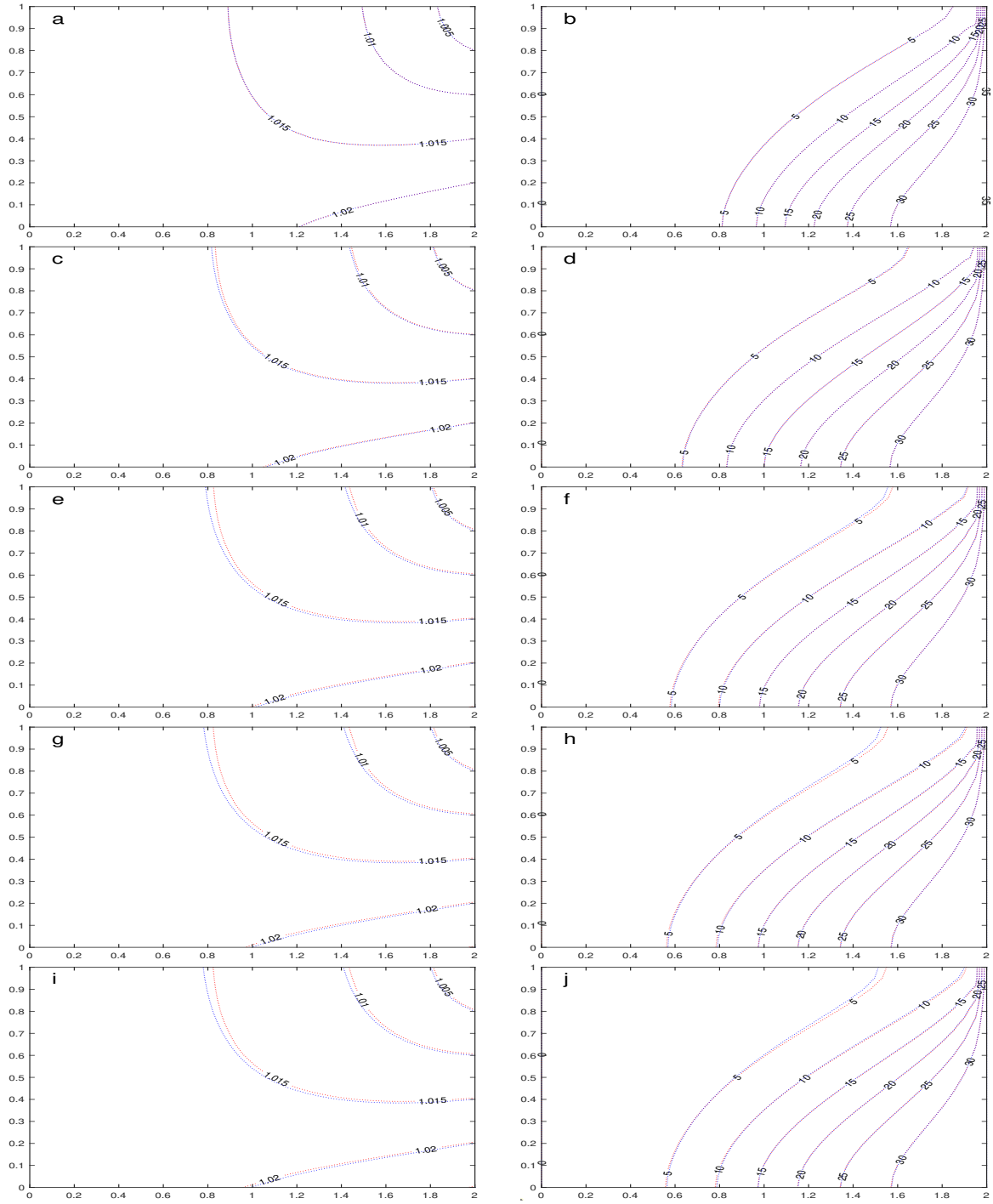

Figure 5.8 Comparison of results between the reduced dimensional (red dash) model with 25 bases and full dimensional (blue dash) model for the homogeneous case. Predicted head distributions (m) at time t = 100 minutes (a), t = 200 minutes (c), t = 300 minutes (e), t = 400 minutes (g), t = 500 minutes (i). Predicted concentration distributions (kg/m^3) at time t = 100 minutes (b), t = 200 minutes (d), t = 300 minutes (f), t = 400 minutes (h), t = 500 minutes (j).

In the homogeneous case, the hydraulic conductivity distribution was taken as 864 m/d in both x-direction (K_{fx}) and z-direction (K_{fz}) for the modified Henry problem. In the heterogeneous case, one random conductivity field and two different zonal conductivity fields were used

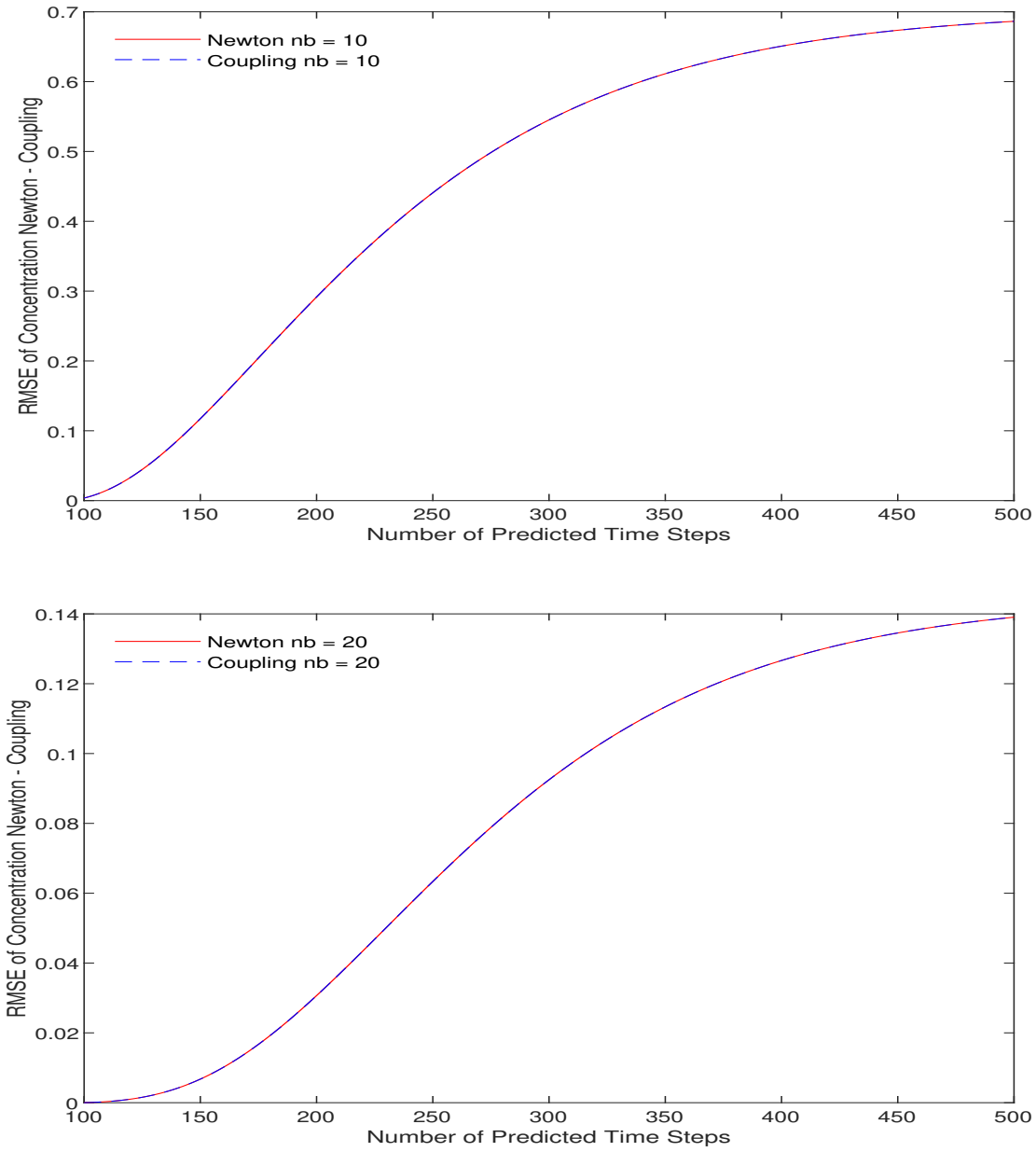

Figure 5.9 RMSE of predicted concentrations between the full dimensional and reduced dimensional models for the homogeneous case using Newton iteration and coupling iteration with 100 snapshots and different bases.

for both reduced dimensional and full dimensional models. All settings, except the hydraulic conductivity, are same for both homogeneous and heterogeneous cases.

In the first case (Case 1), a geostatistical approach was used to generate a hydraulic conductivity field. The anisotropic ratio K_{fx}/K_{fz} was assumed to be 4 over the entire domain, and the distribution of K_f in the x-direction was generated with the Gaussian distribution,

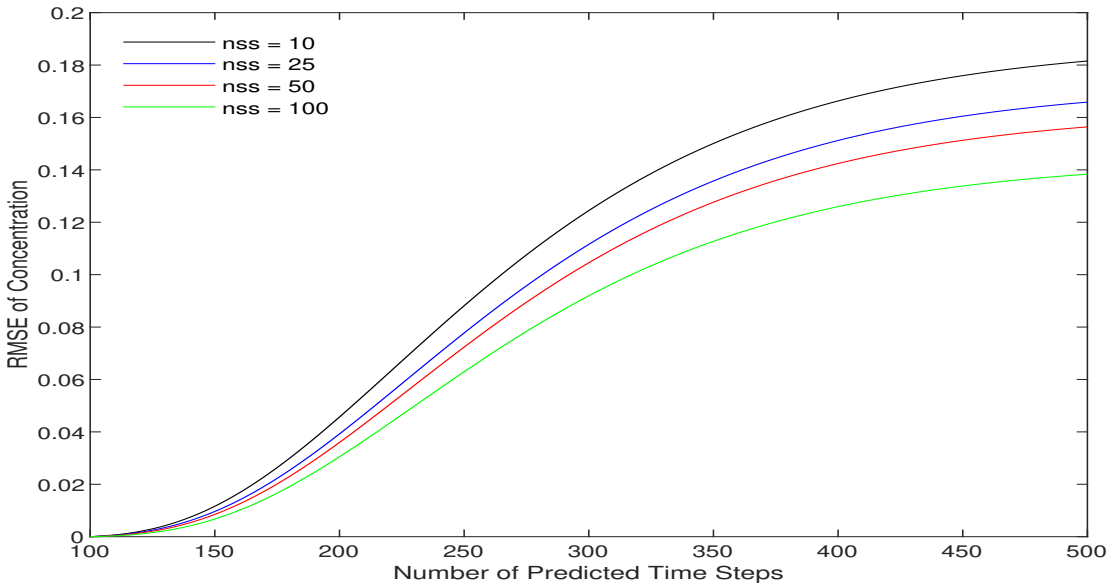

Figure 5.10 RMSE of predicted concentrations between the reduced dimensional and full dimensional models for the homogeneous case using Newton iteration and 25 bases with different number of snapshots.

$N(864, 250)$. In the second case, two different zonal conductivity fields were used, and the conceptual design of the hydraulic conductivity fields are shown in the Figures 5.11. The confined aquifer was divided into five zones, and it is assumed that the anisotropic ratio K_{fx}/K_{fz} is still 4 throughout the domain. In the first pattern (Case 2A), the hydraulic conductivities decrease from top (Zone 1) to bottom (Zone 5). In the second pattern (Case2B), they increase from top (Zone 1) to bottom (Zone 5) in a confined aquifer whose depth is 1 m. Employing 25 bases from 100 snapshots, the reduced dimensional models were run, and simulation results were compared with the full dimensional model results in Figure 5.12, 5.13 and 5.14 for different cases. The CPU times to simulate full dimensional model 500 min in MATLAB with a time step of 1 min is approximately 370 min, 360 min and 340 min for Case 1, Case 2A and Case 2B respectively. The comparison of the CPU times to simulate 500 min for the reduced dimensional model using the Newton and coupling iteration methods are given in the Table 5.2, 5.3 and 5.4. It can be seen that Newton iteration converges faster than coupling iteration for different number of POD bases in each case.

Modified Henry Problem		
Number of Bases (nb)	Computation time (s) with Newton Iteration	Computation time (s) with Coupling Iteration
5	0.1468	0.1865
10	0.2565	0.3335
15	0.4136	0.5593
20	0.6163	0.8606
25	0.9175	1.2466
30	1.2165	1.6942

Table 5.2 Computation times (CPU) of the reduced dimensional model for the heterogeneous case (Case 1) with different nb to simulate 500 time steps

Modified Henry Problem		
Number of Bases (nb)	Computation time (s) with Newton Iteration	Computation time (s) with Coupling Iteration
5	0.1370	0.1992
10	0.2520	0.3363
15	0.3913	0.5438
20	0.5954	0.8256
25	0.8490	1.1560
30	1.1857	1.6260

Table 5.3 Computation times (CPU) of the reduced dimensional model for the heterogeneous case (Case 2A) with different nb to simulate 500 time steps

Modified Henry Problem		
Number of Bases (nb)	Computation time (s) with Newton Iteration	Computation time (s) with Coupling Iteration
5	0.1230	0.1260
10	0.2404	0.2875
15	0.3976	0.5287
20	0.5975	0.8127
25	0.8533	1.1761
30	1.1492	1.6138

Table 5.4 Computation times (CPU) of the reduced dimensional model for the heterogeneous case (Case 2B) with different nb to simulate 500 time steps

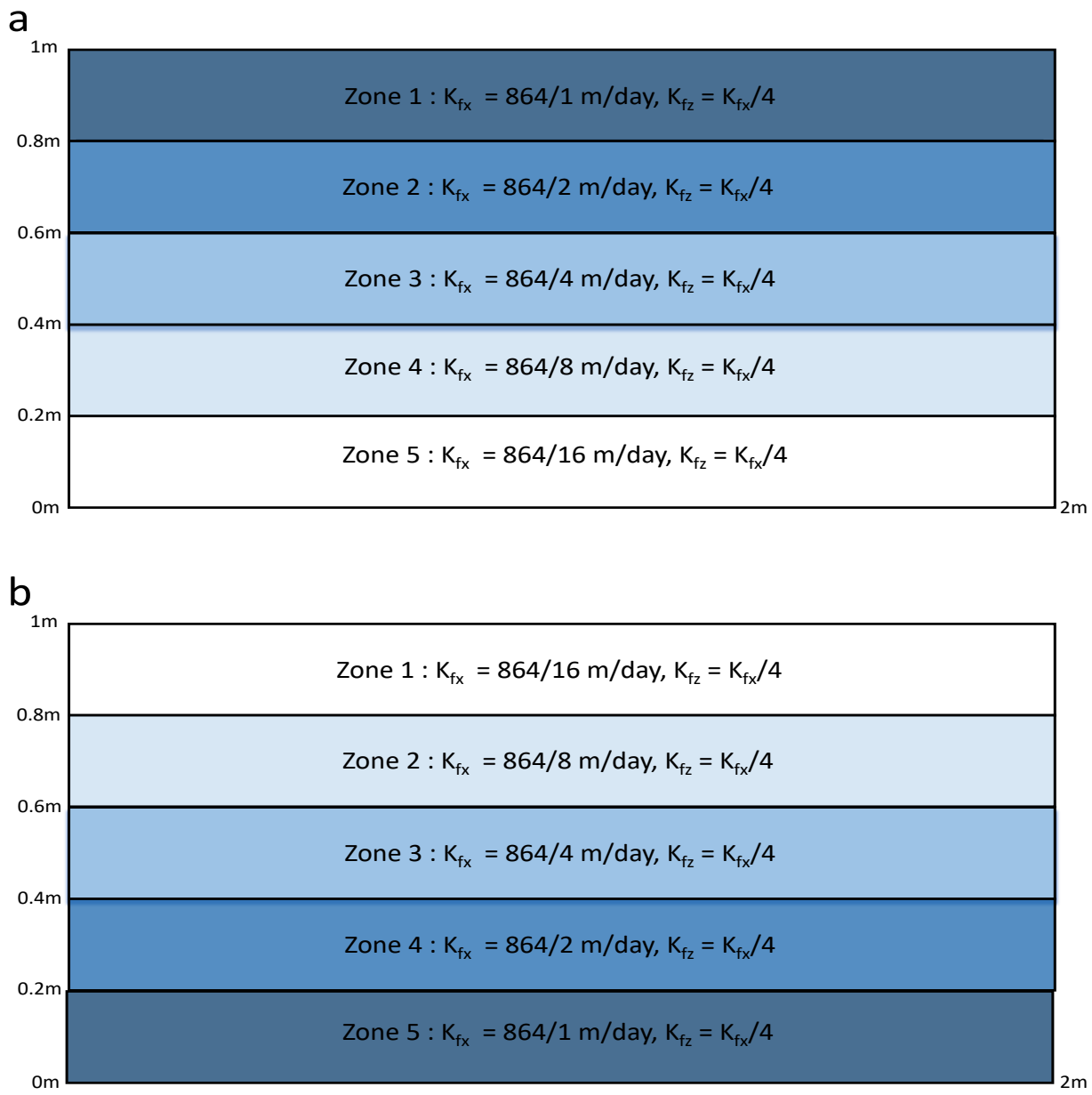

Figure 5.11 Zonal diagrams, cross-sectional view. (a) Hydraulic conductivities decrease by depth; (b) hydraulic conductivities increase by depth.

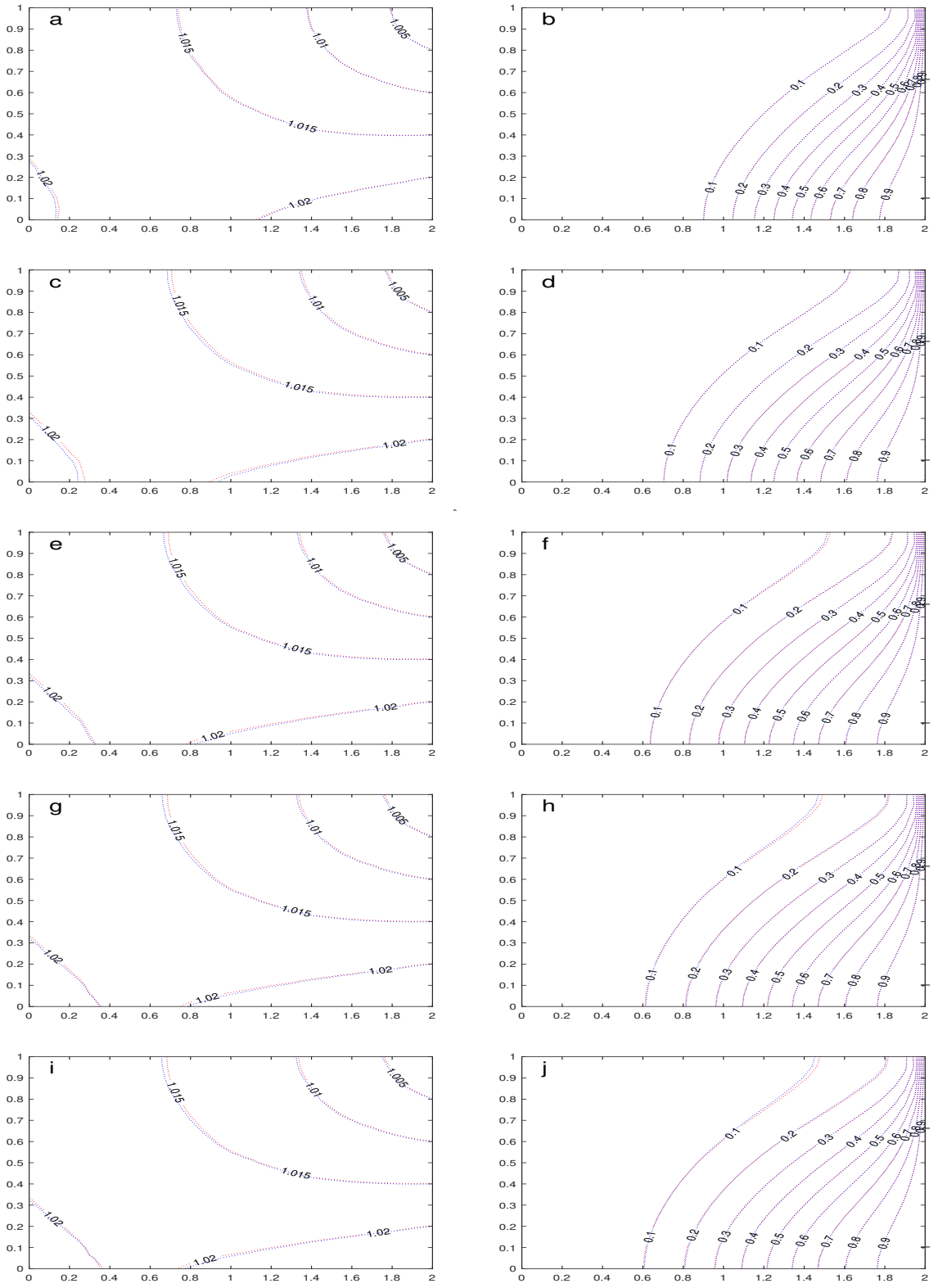

Figure 5.12 Comparison of results between the reduced dimensional (red dash) model with 25 bases and full dimensional (blue dash) model for the heterogeneous case (Case 1). Predicted head distributions (m) at time t = 100 minutes (a), t = 200 minutes (c), t = 300 minutes (e), t = 400 minutes (g), t = 500 minutes (i). Predicted concentration distributions (kg/m^3) at time t = 100 minutes (b), t = 200 minutes (d), t = 300 minutes (f), t = 400 minutes (h), t = 500 minutes (j).

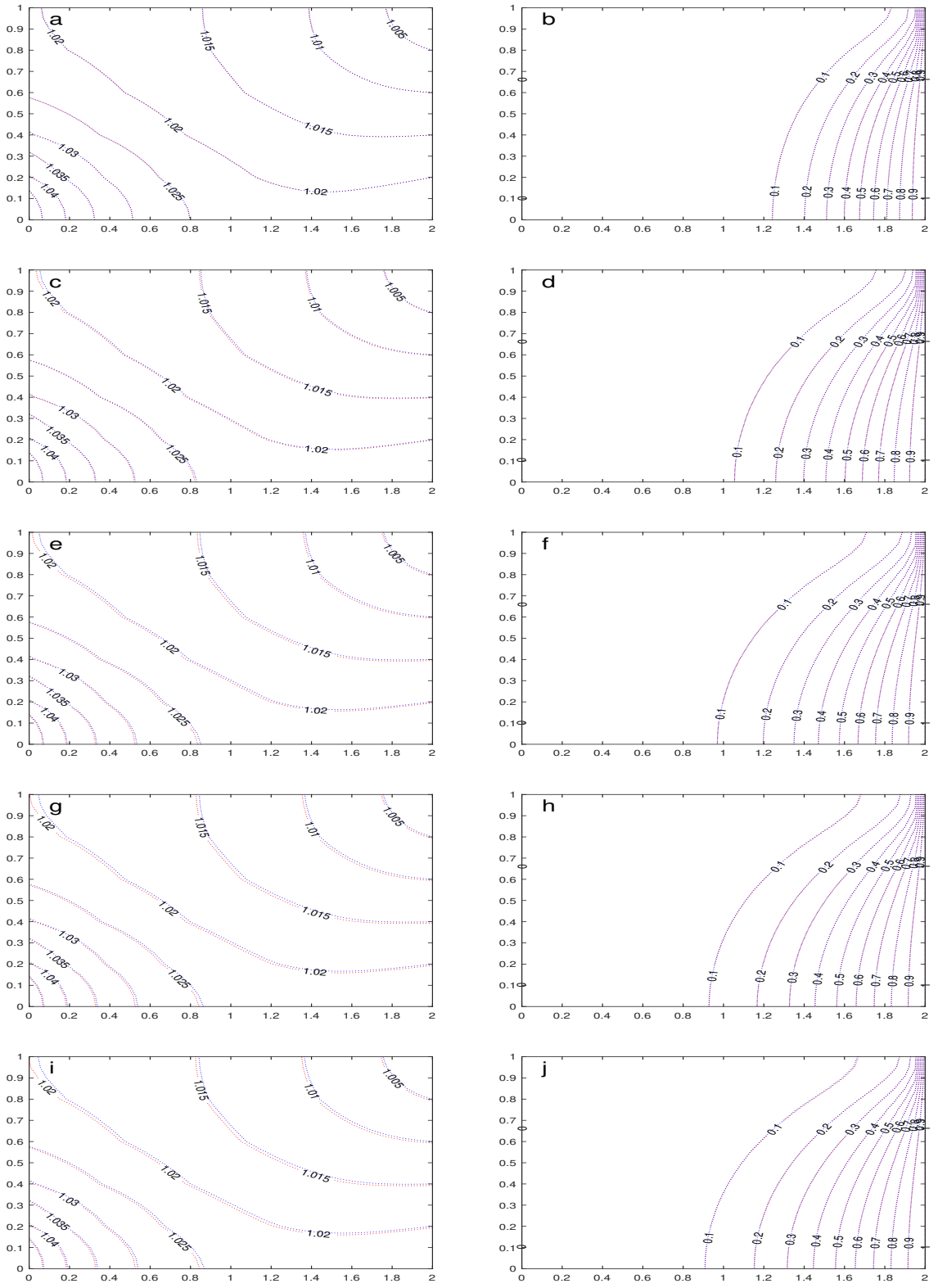

Figure 5.13 Comparison of results between the reduced dimensional (red dash) model with 25 bases and full dimensional (blue dash) model for the heterogeneous case (Case 2A). Predicted head distributions (m) at time t = 100 minutes (a), t = 200 minutes (c), t = 300 minutes (e), t = 400 minutes (g), t = 500 minutes (i). Predicted concentration distributions (kg/m^3) at time t = 100 minutes (b), t = 200 minutes (d), t = 300 minutes (f), t = 400 minutes (h), t = 500 minutes (j).

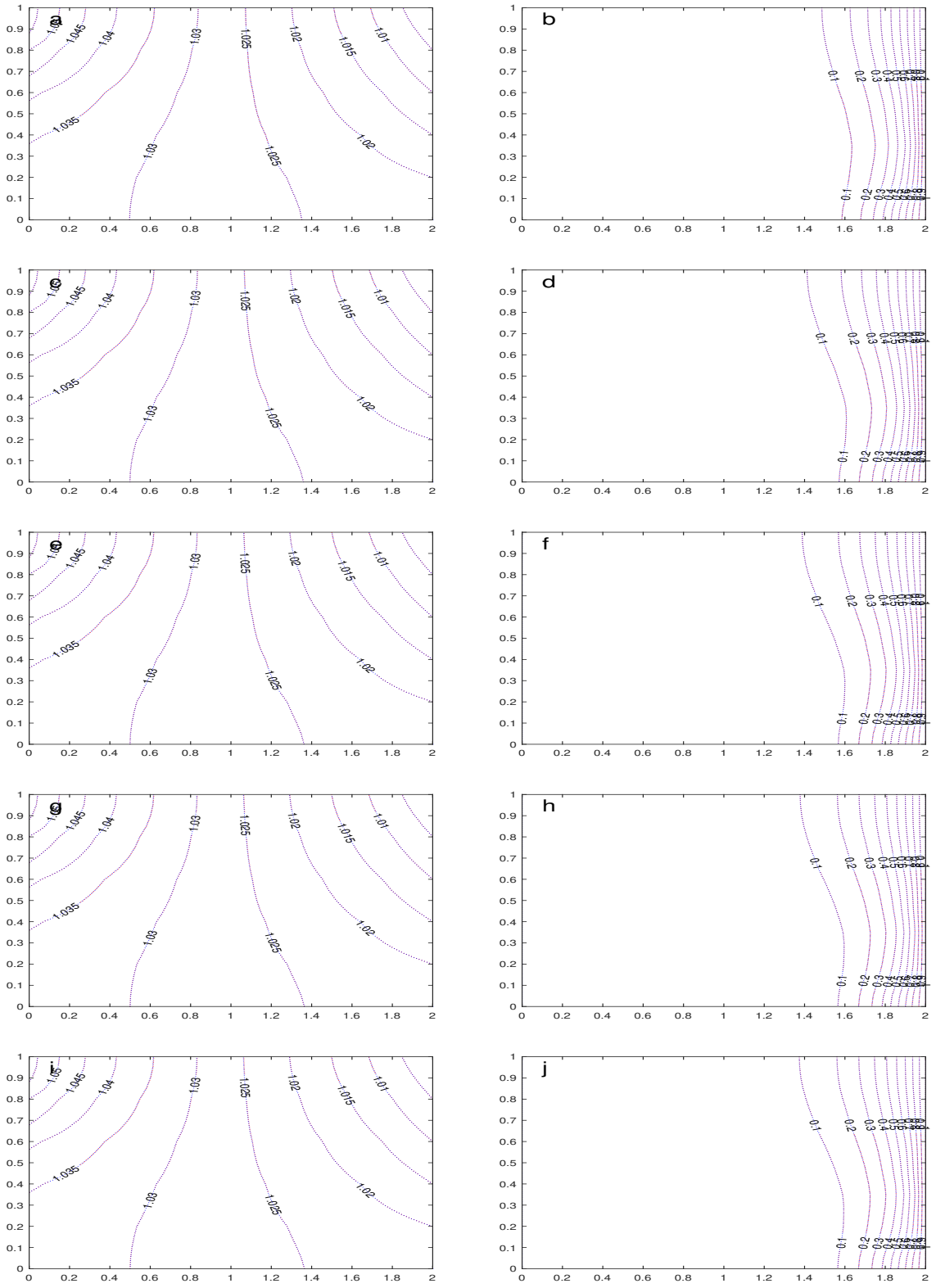

Figure 5.14 Comparison of results between the reduced dimensional (red dash) model with 25 bases and full dimensional (blue dash) model for the heterogeneous case (Case 2B). Predicted head distributions (m) at time t = 100 minutes (a), t = 200 minutes (c), t = 300 minutes (e), t = 400 minutes (g), t = 500 minutes (i). Predicted concentration distributions (kg/m^3) at time t = 100 minutes (b), t = 200 minutes (d), t = 300 minutes (f), t = 400 minutes (h), t = 500 minutes (j).

5.3 The Elder Problem

In the previous section, the modified Henry problem whose internal flow dynamics are mostly determined by the boundary forcing was used to study the accuracy and efficiency of the reduced dimensional model that was generated by the GFEM-POD method with the Newton iteration approach. To test the model under different conditions, the Elder salt convection problem that is highly sensitive to density coupling effects was used. The original Elder problem was generated by Elder [19, 20] and concerns laminar fluid flow that is modeled in the cross-sectional region of a closed rectangular aquifer. The conceptual design of the Elder problem is shown in Figure 5.15. Although there are several other problems that have been used in the literature to benchmark density-dependent groundwater flow codes, both Henry and Elder problems are the most popular ones [58, 59].

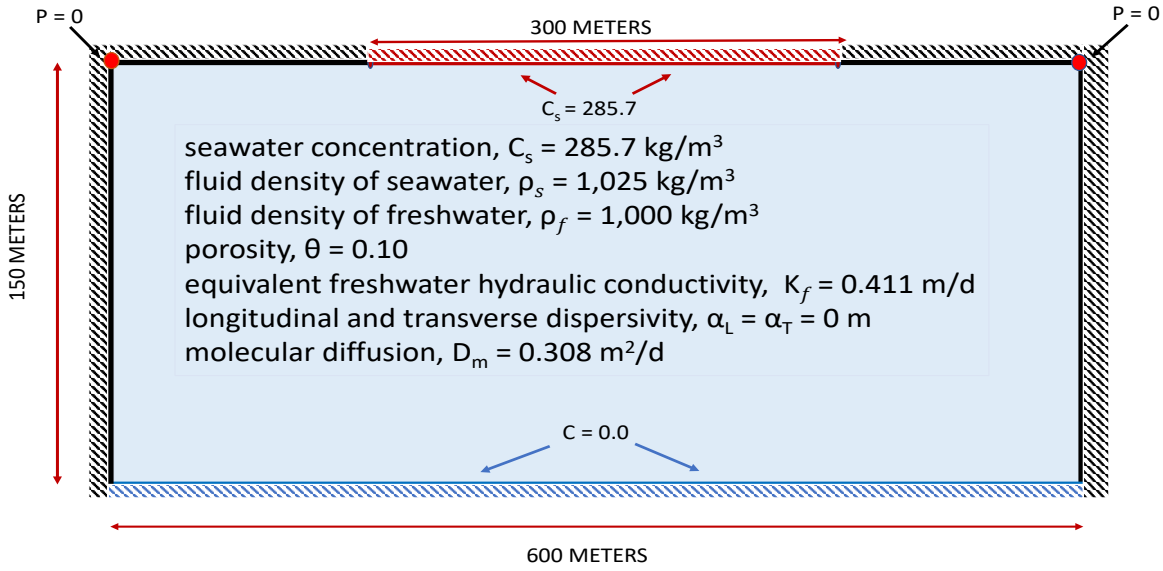

Figure 5.15 Model parameters for the Elder problem

For the Elder problem, the governing equations (2.29) and (2.30) were used considering advection and diffusion without dispersion. To improve the efficiency and to avoid three stable steady state solutions, the molecular diffusion coefficient (D_m) was doubled [35, 37], and a modified Elder problem which we used as the original problem was generated. The domain for this problem was discretized using 7381 nodes and 14400 uniformly aligned linear triangular

elements with the diagonal pointing in the NE-SW direction. To simulate a period of 5 years that is shown in Figure 5.16, a uniform time interval of 5 days was used. The required CPU time to simulate 5 years in MATLAB with a time step of 5 days and a convergence criteria of 10^{-6} kg/m^3 for the fluid concentration between consecutive iterations is approximately 6.5 hours for the modified full dimensional model. The accuracy and efficiency of the reduced

Modified Elder Problem		
Number of Bases (nb)	Computation time (s) with Newton Iteration	Computation time (s) with Coupling Iteration
5	0.2014	0.4565
10	0.3484	0.7723
15	0.6777	1.0322
20	0.9366	1.7275
25	1.0919	2.0653
30	1.7921	2.9371

Table 5.5 Computation times (CPU) of the reduced dimensional model with different nb to simulate 5 years

dimensional model depend on the basis selection, snapshot selection and predicted time length. Since the Elder problem is highly nonlinear, and the error increases gradually as time increases, we testified the reproduction test which is the repeated calculation of the full model. The time period to choose the snapshots is same as the time period used in full dimensional model for the reproduction test. To generate the snapshots, we run the original full dimensional model with a uniform time interval of 5 days for a time period of 5 years (1825 days). 73 snapshots were chosen as one from every 25 days for both concentrations and hydraulic heads. The comparison of the computation times (CPU) of the reduced dimensional models which are generated by the Newton and coupling iteration approaches with different number of bases to simulate 5 years are shown in the Table 5.5. We investigate that the Newton iteration converges faster than coupling iteration under the same convergence criteria. The computation time using the full dimensional model to simulate 5 years is about 6.5 hours. It took about 0.3484 s of CPU time with Newton iteration approach and 0.7723 s of CPU time with coupling iteration with 10 POD modes. Comparison of solute concentration between the reduced dimensional model with Newton iteration approach and the original full dimensional model in the reproduction test is

shown in Figure 5.17. The results of the reduced dimensional model matched more than 99.9% according to the Figure 5.18.

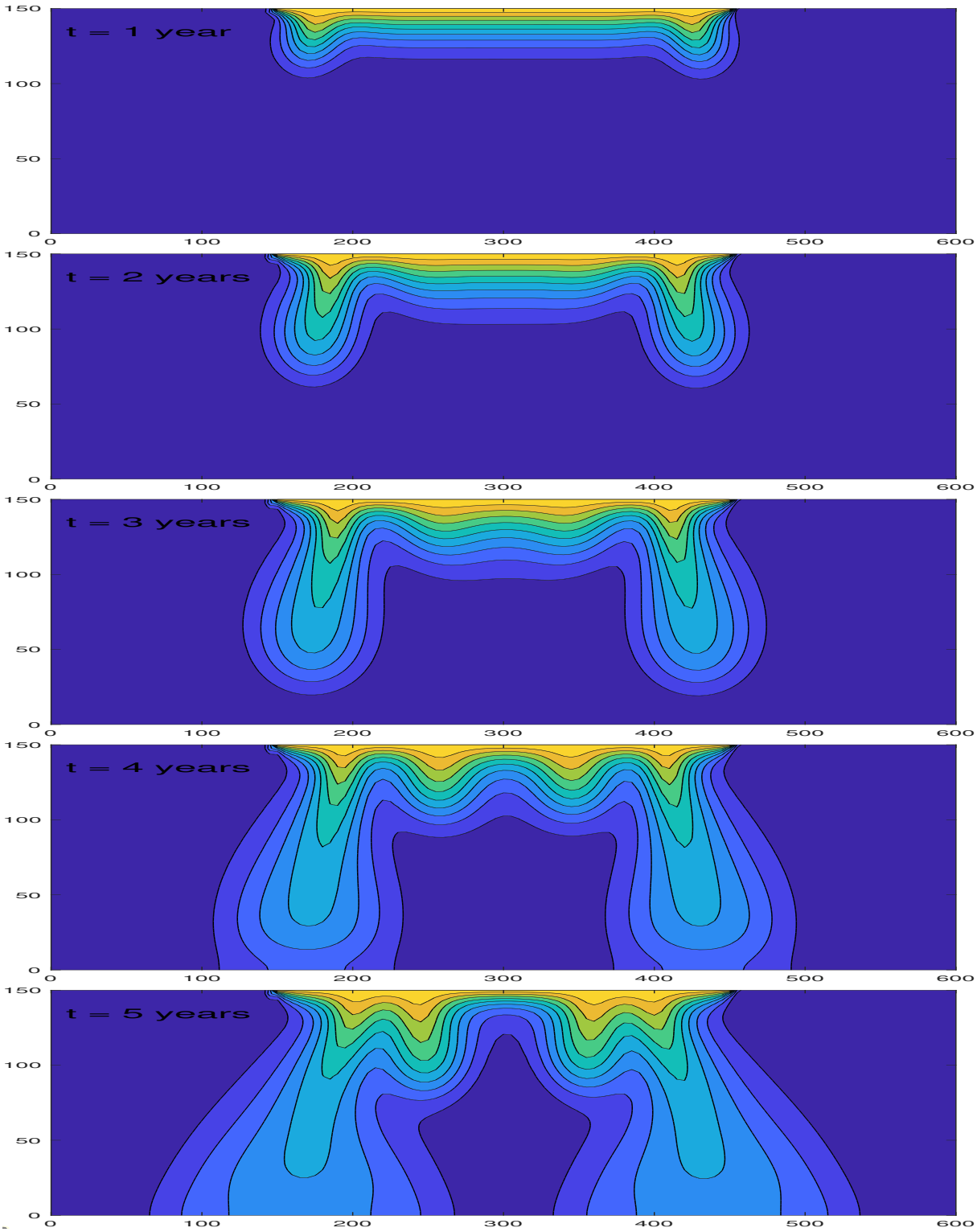

Figure 5.16 Original full dimensional model in the reproduction test.

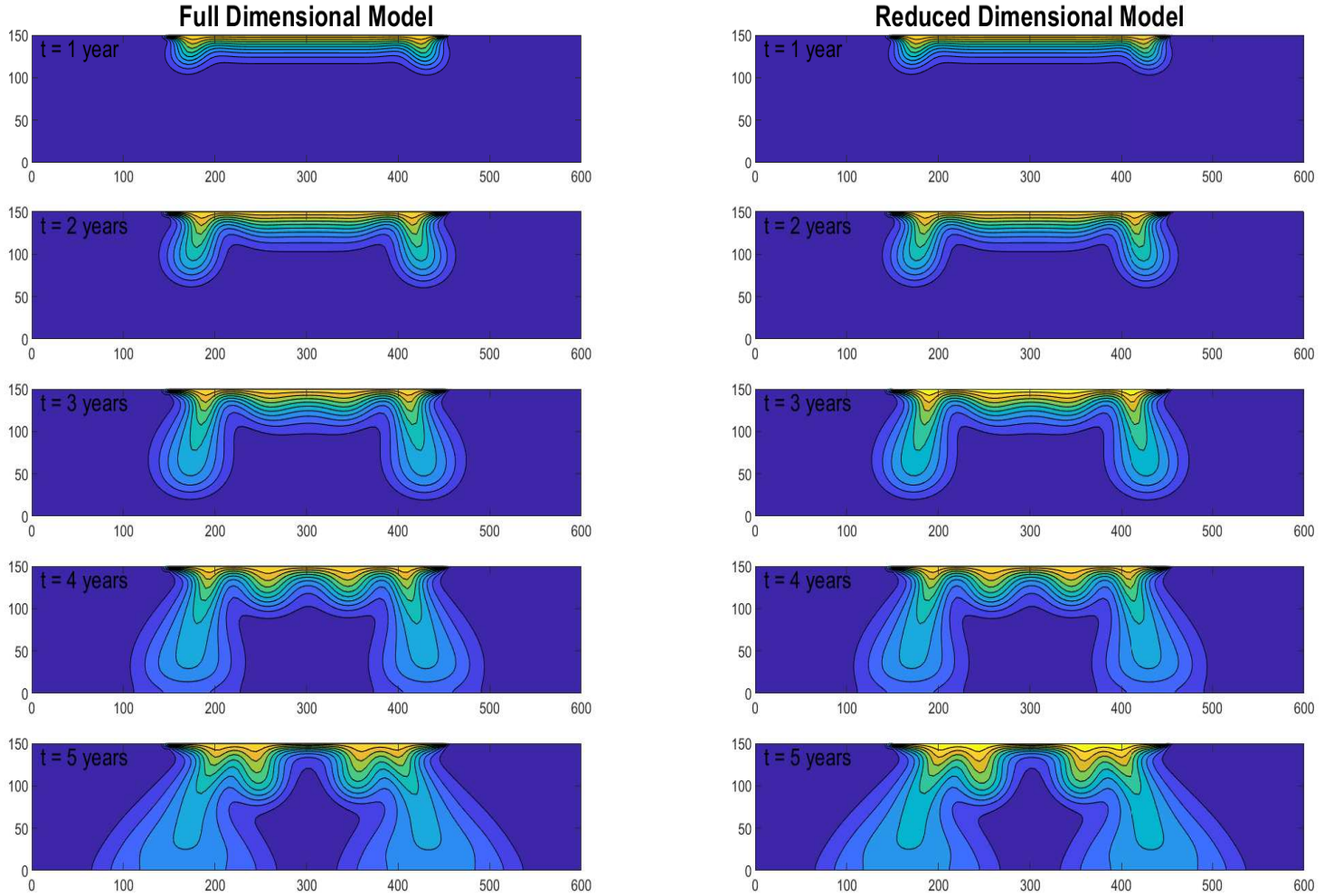

Figure 5.17 Comparison of solute concentration between the reduced dimensional model (right) and the original full dimensional model (left) in the reproduction test.

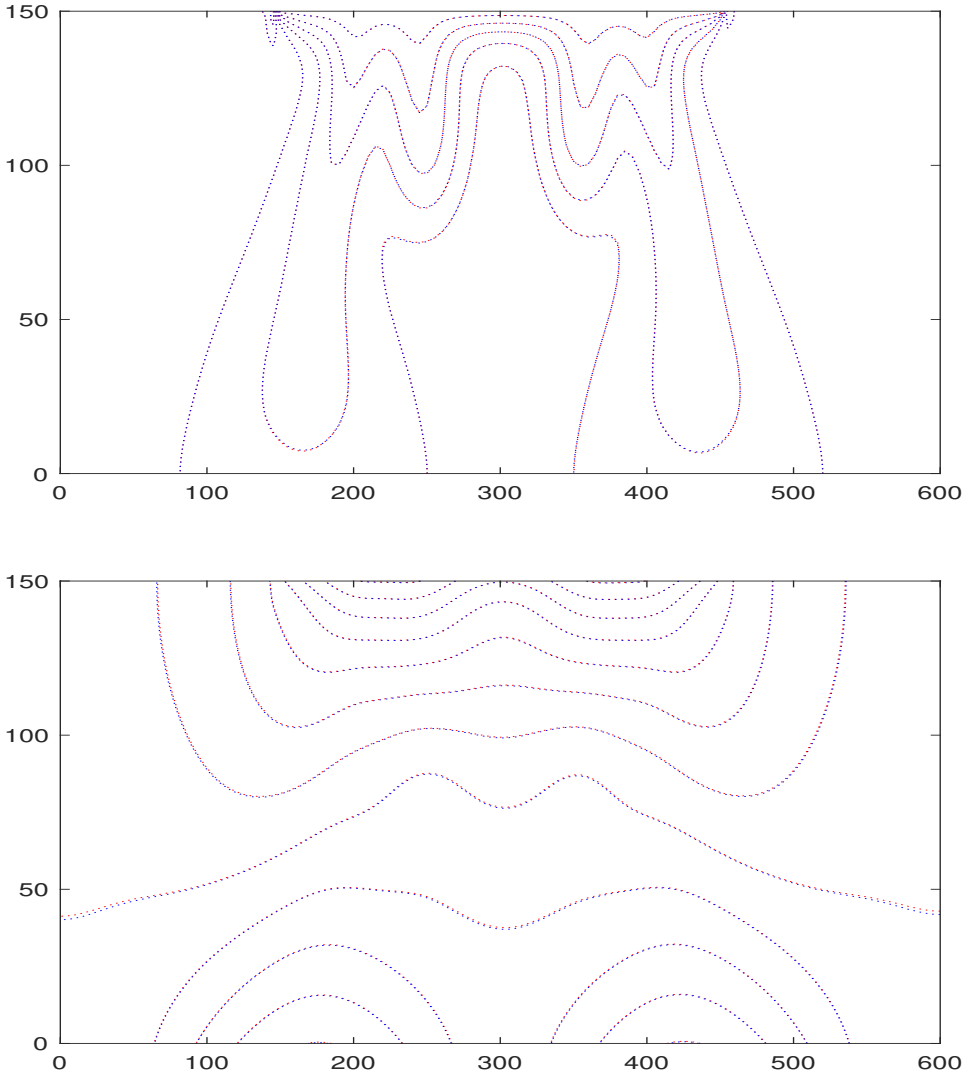

Figure 5.18 Comparison of results between the reduced dimensional (red dash) model with 20 bases and full dimensional (blue dash) model for the modified Elder problem, t=5 years.

Chapter 6

CONCLUSIONS

The VDFST model is a time dependent, nonlinear and coupled dynamical system. If we compare it with constant-density flow and transport model, the numerical discretization of the VDFST requires to be fine, and additional computational loops increase computational time significantly. In this study, we showed that the VDFST model can be solved with at a lower computational cost burden using the GFEM-POD method with the Newton iteration approach.

The accuracy and computational efficiency of the reduced dimensional model have been studied using the Henry and Elder problems, which are two-dimensional examples of the VDFST system. These examples showed that the reduced dimensional model with Newton iteration approach can reproduce and predict the full dimensional model results for both solute concentrations and hydraulic heads very accurately. Also, the study demonstrated that the computation times required for the reduced dimensional model with the Newton iteration approach is less than the computation times required for the reduce dimensional model with the coupling iteration approach.

Another important result is that the accuracy and efficiency of the reduced dimensional model depend strongly on the basis selection, predicted time length and snapshot selection. Therefore, the continued research topic can be optimal basis and snapshot selection to get more accurate and efficient results.

References

[1] Abarca, E., J. Carrera, X. Sanchez-Vila, and M. Dentz [2007]. Anisotropic dispersive Henry problem, Advances in Water Resources, 30, 913-926.

[2] Adomaitis RA. [1995]. RTCVD model reduction: a collocation on empirical eigenfunctions approach. Technical Report T.R. 95–64, Institute of Systems Research.

[3] Aquino, W., J.C. Brigham, C.J. Earls and N. Sukumar [2009]. Generalized finite element method using proper orthogonal decomposition, International Journal for Numerical Methods in Engineering, 79(7): 887-906.

[4] Ataie-Ashtiani, B., R. E. Volker, and D. A. Lockington [1999]. Tidal effects on sea water intrusion in unconfined aquifers, Journal of Hydrology, 216, 17-31.

[5] Bakker, M. [2003]. A Dupuit formulation for modeling seawater intrusion in regional aquifer system, Water Resources Research, 39 (5), 1131.

[6] Bear, J. [1972]. Dynamics of Fluids in Porous Media. Elsevier, New York

[7] Bear J. [1979]. Hydraulics of groundwater. New York:McGraw-Hill.

[8] Bear, J. [1999]. Mathematical modeling of seawater intrusion, Seawater Intrusion into Coastal Aquifers (Bear, J., et al. editors), 127-161, Kluwer Academic Publications.

[9] Bear, J., Cheng, A.D., Sorek, S., Ouazar, D., Herrera, [1999]. I. (eds.) : Theory and Applications of Transport in Porous Media: Seawater Intrusion in Coastal Aquifers - Concepts, Methods and Practices, chap. 5. Kluwer Academic, Dordrecht

[10] Boufadel, M. C. [2000]. A mechanistic study of nonlinear solute transport in a groundwater surface water system under steady state and transient hydraulic conditions, Water Resources Research, 36 (9), 2549-2565.

[11] Burnett, W.C., P.K. Aggarwal, A. Aureli, H. Bokuniewicz, J.E. Cable, M.A. Charette, et al. [2006]. Quantifying submarine groundwater discharge in the coastal zone via multiple methods, Science of the Total Environment, 367 (2-3), 498–543.

[12] Cazemier W, Verstappen RWCP, Veldman AEP. [1998]. Proper orthogonal decomposition and low-dimensional models for driven cavity flows. Physics of Fluids 10: 1685–1699.

[13] Chatterjee, A. [2000]. An introduction to the proper orthogonal decomposition, Current Science, 78(7), 808-817.

[14] Chen, X. S. Akella and I. M. Navon, [2010]. A dual weighted trust-region adaptive POD 4D-Var applied to a Finite-Volume shallow-water Equations Model on the sphere. Submitted for publication to International Journal for Numerical Methods in Fluids.

[15] Ciftci O. [2014]. Model order reduction. Master's thesis, Auburn University.

[16] Di, Z., Z. Luo, Z. Xie, A. Wang and I.M. Navon, [2010], An optimizing implicit difference scheme based on proper orthogonal decomposition for the two-dimensional unsaturated soil water flow equation. Submitted for publication to International Journal for Numerical Methods in Fluids.

[17] Diersch, H.-J.G., and O. Kolditz [2002]. Variable-density flow and transport in porous media: approaches and challenges, Advances in Water Resources, 25(8-12), 899–944.

[18] Dunbar WS, Woodbury AD. [1989]. Application of the Lanczos algorithm to the solution of the groundwater flow equation. Water Resources Research 25(3): 551–558.

[19] Elder JW. [1967a]. Steady free convection in a porous medium heated from below. J Fluid Mech; 27:29–50.

[20] Elder JW. [1967b]. Transient convection in a porous medium. J Fluid Mech; 27:609–23.

[21] Feireisl E., Hilhorst D., Petzeltová H., Taka P. [2016]. Mathematical analysis of variable density flows in porous media. Journal of Evolution Equations, 16, 1-19.

[22] Graham MD, Kevrekidis IG. [1996]. Alternative approaches to the Karhunen–Lo'eve decomposition for model reduction and data analysis. Computers & Chemical Engineering 20(5): 495–506.

[23] Guo, W., and C. D. Langevin [2002]. User's guide to SEAWAT: A computer program for simulation of three-dimensional variable-density ground-water flow. U.S. Geological Survey Techniques of Water-Resources Investigations, Book 6, chapter A7, 77 p.

[24] Henry, H. R. [1964]. Effects of dispersion on salt encroachment in coastal aquifers, U.S. Geological Survey Water-Supply Paper, 1613-C, p. C71-C84.

[25] H. van der Vorst [2008]: Model Order Reduction: Theory, Research Aspects and Applications, pp. 96-109, Springer.

[26] Hoffmann Jørgensen B, Sørensen JN. [2000]. Proper orthogonal decomposition and low-dimensional modelling. ERCOFTAC Bulletin 46: 44–51.

[27] Hooimeijer MA. [2001]. Reduction of Complex Computational Models. Sieca Repro: Delft, The Netherlands.

[28] Hu, B. X., M. M. Meerschaert, W. Barrash, D. W. Hyndman, C. He, X. Li, and L. Guo [2009]. Examining the influence of heterogeneous porosity fields on conservative solute transport. Journal of Contaminant Hydrology, 108: 77-88.

[29] Hu B. X., Cao Y., Zhao W. D., Bao F. [2016]. Identification of hydraulic conductivity distributions in density dependent flow fields of submarine groundwater discharge modeling using adjoint-state sensitivities. SCIENCE CHINA, Earth Sciences, Vol.59 No.4: 770–779.

[30] Khalil, M., S. Adhikari, and A. Sarkat [2007]. Linear system identification using proper orthogonal decomposition, Mechanical Systems and Signal Processing, 21(8), 3123-3145.

[31] Kunisch, K., and S. Volkwein [2002]. Galerkin proper orthogonal decomposition methods for a general equation in fluid dynamics, SIAM Journal on Numerical Analysis, 40(2), 492-515.

[32] Kythe, P. K. and D. Wei [2003]. An introduction to linear and nonlinear finite element analysis: a computational approach, Birkhauser, Boston, 445pp.

[33] Langevin, C.D., W.B. Shoemaker, and W. Guo [2003]. MODFLOW-2000, the U.S. Geological Survey modular ground-water model–documentation of the SEAWAT-2000 version with the Variable-Density Flow process (VDF) and the Integrated MT3DMS Transport process (IMT), U.S. Geological Survey Open-File Report 03-426, 43 p.

[34] Langevin, C.D. [2003]. Simulation of submarine ground water discharge to a marine estuary: Biscayne Bay, Florida, Ground Water, 41(6), 758–771.

[35] Li, X., B. X. Hu, W. C. Burnett, I. R. Santos, and J. P. Chanton [2009]. Submarine ground water discharge driven by tidal pumping in a heterogeneous aquifer, Ground Water, 47(4): 558-568.

[36] Li, X. [2010]. Model Simulation and Reduction of Variable-density Flow and Solute Transport using Proper Orthogonal Decomposition. Ph.D. Thesis, Department of Earth, Ocean and Atmospheric Science, Florida State University, Tallahassee, Florida.

[37] Li X., Chen X., Hu B. X. and Navon I. M [2013]. "Model Reduction of A Coupled Numerical Model Using Proper Orthogonal Decomposition" *Journal of Hydrology* 507, pp. 227-240

[38] Lumley, J.L., [1967]. In: Yaglom, A., Tatarski, V. (Eds.), Atmospheric Turbulence and Radio Wave Propagation. Nauka, Moscow, pp. 166–178.

[39] Martin, J.B., J.E. Cable, P.W. Swarzenski and M.K. Lindenberg [2004]. Enhanced submarine ground water discharge from mixing of pore water and estuarine water, Ground Water, 42(7), 1000-1010.

[40] McDonald MG, Harbaugh AW. [1988]. A modular three-dimensional finite-difference groundwater flow model. US Geological Survey, Open- File Report 83–875, Book 6, Chapter A1.

[41] Navon, I. M. [1979]. Finite Element Simulation of the Shallow-Water Equations Model on a Limited- Area Domain, Appl. Math. Modeling, 3, 337-348

[42] Newman AJ. [1996a]. Model reduction via the Karhunen-Lo'eve expansion. Part I: an exposition. Technical Report T.R. 96–32, Institute of Systems Research.

[43] Newman AJ. [1996b]. Model reduction via the Karhunen-Lo'eve expansion. Part II: some elementary examples. Technical Report T.R. 96–33, Institute of Systems Research.

[44] Pinnau, R. [2008]. Model reduction via proper orthogonal decomposition, to appear in W.H.A. Schilder.

[45] T. J. Povich, C. N. Dawson M. W. Farthing, C. E. Kees [2013]. Finite element methods for variable density flow and solute transport. Comput Geosci 17:529–549.

[46] Reis, T. and T. Stykel [2007]. Stability analysis and model order reduction of coupled systems, Mathematical and Computer Modeling of Dynamic Systems, 13(5):413-436.

[47] Robinson, B.A., Z. Lu, and D. Pasqualini [2009]. Simulating solute transport in porous media using model reduction techniques, preprint submitted to Advances in Water Resources.

[48] Sahuquillo A. [1983]. An eigenvalue numerical technique for solving unsteady linear groundwater models continuously in time. Water Resources Research 19: 87–93.

[49] Sanz, E., and C. I. Voss [2006]. Inverse modeling for seawater intrusion in coastal aquifers: Insights about parameter sensitivities, variances, correlations and estimation procedures derived from the Henry problem, Advances in Water Resources, 29, 439-457.

[50] Schincariol, R.A., and F.W. Schwartz [1990]. An experimental investigation of variable density flow homogeneous and heterogeneous media, Water Resources Research, 26(10), 2317–2329.

[51] Segol G, Pinder GF, Gray WG. [1975]: A Galerkin-finite element technique for calculating the transient position of the saltwater front. Water Resour Res; 11:343–7.

[52] Segol, G. [1993]. Classic groundwater simulations: Proving and improving numerical models, Englewood Cliffs, N.J., PTR Prentice Hall, 531 p.

[53] Shikaze, S. G.., E. A. Sudicky, and F. W. Schwartz [1998]. Density-dependent solute transport in discretely-fractured geologic media: is prediction possible? Journal of Contaminant Hydrology, 34(3), 273-291.

[54] Shoemaker, W.B. [2004]. Important observations and parameters for a salt water intrusion model, Ground Water, 42(6), 829-840.

[55] Siade, A. J. M. Putti and W. W.-G. Yeh [2010]. Snapshot selection for groundwater model reduction using proper orthogonal decomposition, Water Resources Research, 46, W08539, 13 PP., doi:10.1029/2009WR008792.

[56] Simmons, C.T., T.R. Fenstemaker, and J.M. Sharp [2001]. Variable-density groundwater flow and solute transport in heterogeneous porous media: approaches, resolutions and future challenges, Journal of Contaminant Hydrology, 52(1-4), 245–275.

[57] Simmons, G. M. Jr [1992]. Importance of submarine groundwater discharge (SGWD) and seawater cycling to material flux across sediments/water interfaces in marine environments, Marine Ecology Progress Series, 84, 173-184.

[58] Simpson, M.J. and T.P. Clement [2003]. Theoretical analysis of the worthiness of Henry and Elder problems as benchmarks of density-dependent groundwater flow models, Advances in Water Resources, 26:17-31.

[59] Simpson, M.J. and T.P. Clement [2004]. Improving the worthiness of the Henry problem as a benchmark for density-dependent groundwater flow models, Water Resources Research, 40, W01504.

[60] Sirovich L. [1987]. Turbulence and the dynamics of coherent structures; part I: coherent structures. Quarterly Applied Mathematics 45(3): 561–571.

[61] Vermeulen PTM, Heemink AW, te Stroet CBM. [2001]. Model reduction in groundwater hydrology. In Final Proceedings of the International Conference on Modelling and Simulation, Canberra, Australia, vol. 1; 407–412.

[62] Vermeulen, P. T. M., A. W. Heemink, and C. B. M. te Stroet [2004a]. Low-dimensional modeling of numerical groundwater flow, Hydrological Process, 18(8), 1487-1504

[63] Vermeulen, P. T. M., A. W. Heemink, and C. B. M. te Stroet [2004b]. Reduced models for linear groundwater flow models using empirical orthogonal functions, Advances in Water Resources, 27(1), 57-69.

[64] Vermeulen, P. T. M., A. W. Heemink, and J. R. Valstar [2005]. Inverse modeling of groundwater flow using model reduction, Water Resources Research, 41(6), W06003.

[65] Vermeulen, P. T. M., and A. W. Heemink [2006a]. Model-reduced variational data assimilation, Monthly Weather Review, 134(10), 2888-2899.

[66] Vermeulen, P. T. M., C. B. M. te Stroet, and A. W. Heemink [2006b]. Model inversion of transient nonlinear groundwater flow model using model reduction, Water Resources Research, 42(9), W09417.

[67] Voss, C.I. [1984]. A finite-element simulation model for saturated-unsaturated, fluid-density dependent ground-water flow with energy transport or chemically-reactive single-species solute transport, U.S. Geological Survey Water-Resources Investigation Report 84-4369, 409 p.

[68] Voss, C.I. and Souza W.R.[1987]. Variable density flow and solute transport simulation of regional aquifers containing a narrow freshwater-saltwater transition zone, Water Resources Research, 23(10): 1851-1866.

[69] Voss, C. I., and A. M. Provost [2002]. SUTRA: A model for saturated-unsaturated, variable density ground-water flow with solute or energy transport, U.S. Geological Survey Water-Resources Investigations Report 02-4231.

[70] Zhang K, Woodbury AD. [2000a]. The Arnoldi reduction technique for efficient direct solution of radionuclide decay transport in dual-porosity media. Journal of Contaminant Hydrology 44: 387–416.

[71] Zhang K, Woodbury AD. [2000b]. Application of the Lanczos algorithm to the simulation of groundwater flow in dual-porosity media. Advances in Water Research 23: 579–589.